ASTROBIOLOGY
Volume 00, Number 00, 2026
Mary Ann Liebert, A Part of Sage

DOI: 10.1177/15311074261417883

Biosignature Detection and Preservation in Lake Salda Microbialites Under Simulated Martian Conditions

Connor J. Ballard,[1] Louisa J. Preston,[1] Lewis R. Dartnell,[1,2] Eva Mateo-Marti,[3] Catherine Regan,[4] and Andrew Coates[1]

Abstract

The alteration of martian deposits under extreme surface conditions remains a key challenge for their mineral-organic interpretation and paleoenvironmental reconstruction. This study investigates the spectral detection and alteration of mineral-organic signatures in Lake Salda hydromagnesite microbialites under martian sublimation and radiation (UV) conditions. Samples were analyzed using visible near-infrared and Fourier transform infrared (FTIR) spectroscopy, then sublimated via lyophilization and exposed to UV radiation in the Planetary Atmospheres and Surfaces Simulation Chamber. Sublimation reduced the intensity of water and carbonate vibrations and enhanced CH_2 ν_3 and PO_2^- ν_3 organic features; this demonstrated that interstitial water sublimation may reduce O–H spectral noise, improve organic visibility, and reveal volatile sublimation patterns for future Mars rovers, such as Rosalind Franklin. In a three-sol (74 h) simulation of martian UV radiation (200–400 nm) under 7 mbar of CO_2, FTIR spectral intensity was reduced, and organic CH_2 ν_3 and PO_2^- features were significantly degraded. These findings reveal spectral alterations under martian surface conditions and highlight organic biosignature vulnerability at equatorial latitudes, informing preservation protocols for future missions. Key Words: Mg carbonates—Hydromagnesite—Jezero crater—Mars—Spectral biosignatures—Rosalind Franklin. Astrobiology 00, 000–000.

1. Introduction

Terrestrial carbonate phases are often associated with the preservation of biosignatures due to their microbially induced precipitation mechanisms (Kawaguchi and Decho, 2002a, 2002b; Braissant et al., 2003; Dupraz et al., 2004; Dupraz and Visscher, 2005; Visscher and Stolz, 2005; Dupraz et al., 2009; Balci et al., 2020), their ability to encapsulate microbial matter during mineral growth (Dupraz et al., 2009; Melim et al., 2016), and their relative geochemical stability over time, which allows organic features to persist even after diagenesis (Cousins et al., 2020). Biosignatures can form in several distinct ways within terrestrial carbonates. Morphological features include domal, columnar, or laminated macrostructures formed through microbially mediated sediment trapping (Riding, 2000; Allwood et al., 2006). Mineralogical signatures may involve the precipitation of specific carbonate phases, such as dolomite or hydromagnesite, influenced by microbial processes and distinct from abiotic forms (Vasconcelos et al., 1995; Bontognali et al., 2010), and textural evidence can be identified when microbial biofilms, such as EPS (extracellular polymeric substances), influence crystal nucleation and growth (Dupraz et al., 2004; Yin et al., 2020). Organo-geochemical features are varied but include the formation of biomineral–organic complexes, specifically calcium bound to cell surfaces (Benning et al., 2004), the preservation of lipid biomarkers (Pagès et al., 2015; Balci et al., 2020), and isotopic signatures, such as calcium isotope fractions (Bradbury et al., 2020) or stable carbon and oxygen isotope ratios in microbially mediated carbonate precipitates (Balci et al., 2020).

On Mars, the harsh conditions and poorly known past surface processes make biosignature recognition difficult. The early Viking missions (Margulis et al., 1979) documented a hostile surface environment with high UV radiation and low water availability and temperatures, which are exacerbated by oxidizing surface conditions and a thin CO_2-rich atmosphere (Grady, 2007; Direito et al., 2012). At Jezero crater, UV radiation, particularly UVC (Gil-Lozano et al., 2020), coupled with sublimating surface pressures (7.5 mbar) (Savijärvi et al., 2023) and temperatures (190–270 K) (Zorzano et al., 2024), can be deleterious for potential biomolecules preserved within the crater deposits (Stalport et al., 2009; Gil-Lozano et al., 2020). Cosmic and solar ionizing radiation may also affect the potential viability of radioresistant cells up to ~2 m depth (Dartnell et al., 2007a, 2007b),

[1]Department of Space and Climate Physics, Mullard Space Science Laboratory (MSSL), University College London, Dorking, UK.
[2]Department of Life Sciences, University of Westminster, London, UK.
[3]Centro de Astrobiología (CAB) INTA-CSIC, Madrid, Spain.
[4]Department of Physics and Astronomy, West Virginia University, Morgantown, West Virginia, USA.

which could be particularly damaging for biomolecules in the top 5–10 cm of a geological outcrop that exceeds 300 million years (Pavlov et al., 2012). Mars UV radiation exposure experiments have shown that the longer the exposure time, the more deleterious the damaging effects of the radiation are; a 469-day simulation of the martian radiation environment that compared different radiation types showed that it strongly changed the Raman spectral signal of seven known biomolecules in a comparative study where only minor changes occurred in the samples shielded from UV radiation (Baqué et al., 2022). UV radiation is known to penetrate >500 μm in a variety of Mars analog substrates, including gypsum, kaolinite, basaltic martian simulant, and welded tuff in the wavelength range of 220–400 nm (Carrier et al., 2019). Given this, it may be possible to analyze samples 1–2 mm deep that are unaffected by UV radiation penetration. While the ExoMars Rosalind Franklin rover's 2 m drill will be able to access a significant depth (Vago et al., 2017), the Perseverance rover can only drill up to 76 mm (Moeller et al., 2021), yet still potentially evade the worst of UV degradation. It is, therefore, imperative to understand how UV radiation influences shallow subsurface samples, in order to obtain an accurate interpretation of carbonate on the martian surface.

Evaporative models of Mg precipitate accumulation in playas or lakes require large volumes of water to flow through the system (Wood and Sanford, 1990), which indicates that magnesite and hydromagnesite accumulations result from long-term water availability (Scheller et al., 2021). Nearshore terrace deposits can also accumulate more rapidly through localized increases in alkalinity and pH, initiated from the biological consumption of CO_2, which is more favorable for Mg precipitation and increases accumulation in the lake margins (Balci et al., 2020; Gunes et al., 2022, 2023). Given that terrestrial hydromagnesite can occur through both biotic and abiotic pathways, investigations at Jezero crater must first exclude abiotic formation processes. Nevertheless, terrestrial Mars analog sites with marginal hydromagnesite accumulation provide valuable insights into abiotic and potentially biogenic formation mechanisms. These analogs are invaluable for constraining mineralogical and environmental controls that influence the preservation of biosignatures and their interpretation. Here, we expose martian carbonate analog samples to the environmental regime of the martian surface—very low atmospheric pressure and temperature, and intense UV radiation—to study the impact it has on the detectability of mineral spectral features and potential biosignatures. This research informs the analysis of current martian surface samples as well as those that will be retrieved from greater depths, which may subsequently be exposed to martian surface conditions for extended periods.

1.1. Site description

An excellent analog for Mg carbonate precipitation in an ancient Jezero crater can be found at Lake Salda, an alkaline lake (pH > 9) located in Burdur, SW Turkey, which is $\sim$45 km^2 in surface area and up to 200 m deep (Braithwaite and Zedef, 1996). The lake system today has limited water inflow from precipitation, groundwater, and ephemeral streams, with no water outlet except via evaporation, and is therefore an endorheic basin (Davraz et al., 2019; Gunes et al., 2023). The water chemistry is thought to remain seasonally constant with high Mg content (51–408.5 mg/L) and decreasing abundances of Na, Si, Ca, and K, respectively (Balci et al., 2020). The ultramafic watershed contains harzburgite, metamorphosed to lizardite in places, as the dominant rock that underlies the lake basin (Gunes et al., 2023) and forms part of the Marmaris peridotite ophiolite complex (Xu et al., 2020). Meteoric waters that flow through the ultramafic watershed and alluvial fan deltas NW, SW, and SE of the lake facilitate Mg enrichment and increase the alkalinity of the lake water (Kazanci et al., 2004).

Precipitation of Mg here is promoted by living microbial mats, which form abundant stromatolites and microbialites of various morphologies within the littoral zone (Balci et al., 2020). Microbialites in this context are defined as carbonate structures influenced by benthic microorganisms, which are documented to grow in the shallow (<1 m) and deep ($\sim$15 m) waters of Lake Salda with morphological, mineralogical, and microbial diversity (Gunes et al., 2023). Previous investigations of Lake Salda deposits have characterized the geological context (Braithwaite and Zedef, 1996, 1994) and studied the distribution of sedimentary lipid biomarkers (Kaiser et al., 2016). More recent studies have used orbital and visible near-infrared (VisNIR) spectroscopy to understand carbonate spectral properties through the lens of the Perseverance rover (Garczynski et al., 2019, 2020, 2021, 2023) and have improved our understanding of microbial processes on microbialite formation through isotopic, mineralogical, and microscopic analyses (Balci et al., 2020), and Raman spectroscopy (Yılmaz and Unsalan, 2022). This study represents the first attempt to analyze Lake Salda microbialites using Fourier transform infrared (FTIR) and VisNIR spectroscopy to determine the potential for organic biosignature detection, preservation, and degradation before and after exposure to simulated martian surface conditions.

2. Method

Samples in this project were collected during fieldwork conducted in May 2023. The sample suite included microbialites actively growing from beneath the shoreline (subaqueous) and on the beachfront (subaerial), and preserved in ancient terrace structures, interpreted as relics of past shoreline depositional zones. Beach detrital sediment and hydromagnesite muds were also collected from various locations around the lake. This project focuses on Mid- and Lower-Terrace Microbialites (MTM and LTM) of the Eastern tiered terrace system, Locality 5, and the Salda Gölü North Microbialite (SGNM) with high organic content, from the NW flank of Lake Salda, Locality 2 (Fig. 1 and Table 1).

2.1. Instrumentation

Microscopy was undertaken with an AmScope ME580 microscope housed at the Mullard Space Science Laboratory (MSSL), used to visualize textural differences between samples. Photos were taken with the AmScope MU1803 18 MP Aptina Colour CMOS microscope camera, and the images were captured using the default AmScope imaging software. Microscopy was carried out on whole, unpowdered microbialites to preserve the structural and textural characteristics.

Visible and near-infrared spectroscopy covering the range of 350–2500 nm was applied to understand mineralogical constituents of the microbialites and which biosignatures, if

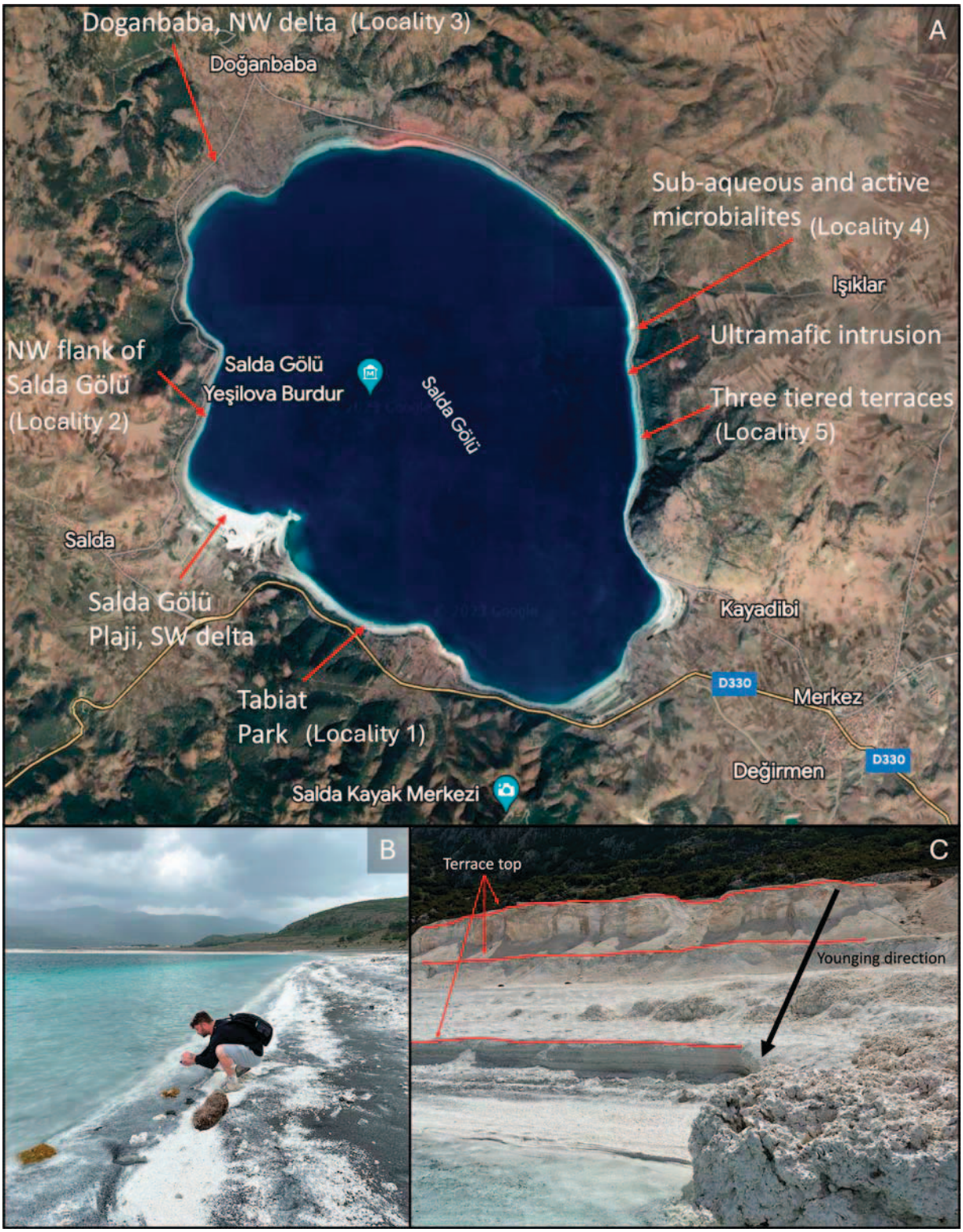

FIG. 1. **(A)** Map of Lake Salda with sampled locations and key localities 1–5. **(B)** Locality 2, NW flank of Lake Salda, sample site of the SGNM. **(C)** Locality 5, East Lake Terraces, the sample location of the Lower- and Mid-Terrace Microbialites. The younging direction and three distinct terrace units are marked. SGNM, Salda Gölü North Microbialite.

any, were detectable within these wavelengths. Analyses were conducted on an ASD RxSpec 700z VisNIR reflectance spectrometer, housed at the University of Westminster (UOW). Analysis was carried out on representative powdered subsamples that reflected the mineralogical and textural characteristics of microbialites A–C (Fig. 2); subsamples were placed into a glass sampling tray. Further analyses on the whole, unpowdered microbialite were collected using a fiber

Table 1. Study Samples with the Respective Localities and Coordinates

Locality	*Locality name*	*Sample name*	*Coordinate (latitude, longitude)*
2	NW Flank of Lake Salda	Salda Gölü North Microbialite (SGNM)	37.54781, 29.64482
5	East Lake Terraces	Mid-Terrace Microbialite (MTM)	37.54621, 29.71873
5	East Lake Terraces	Lower-Terrace Microbialite (LTM)	37.54621, 29.71873

optic illuminator, which enabled sampling of specific regions of interest (ROI), in this case, areas with and without extensive microbial coverage.

The primary mode of investigation was FTIR spectroscopy covering the range of 4100–500 cm^{-1}, applied here to constrain fundamental IR vibrations of the comprising mineralogy, hydration changes in the hydrous magnesium carbonate phases (hydromagnesite) between the initial samples and those subjected to martian conditions, and organic band absorptions that infer biosignature preservation and degradation potential in hydromagnesite deposits. Analyses were conducted across two instruments: a portable Agilent 4300 FTIR spectrometer with diamond ATR attachment, 4 cm^{-1} resolution, housed at MSSL, used for initial analyses; a bench-top Perking Elmer Spectrum Two FTIR spectrometer with UATR2 attachment, housed at the UOW, used for rapid analysis postlyophilization. Analyses for these instruments were conducted on representative powdered subsamples, selected to reflect the textural and mineralogical characteristics of microbialites A–C (Fig. 2).

Historically, lyophilization (freeze-drying) has been used as a drying process in the food and pharmaceutical industries, among wider medicinal applications (Kasper et al., 2013). In this study, lyophilization simulated martian surface sublimation to evaluate the impact on hydromagnesite microbialites and their mineralogical and organic features. It enabled the removal of interstitial water from the samples, which can interfere with spectroscopic interpretations. Simulations were performed using a Labconco Freezone 12L Lyophilizer housed at UOW. Sample weights were taken before and after lyophilization to establish water loss (%), and all samples were placed in a freezer at −20°C for a minimum of 20 min before testing to bring samples closer to the drying temperature. Samples were exposed to temperatures and pressures of −60°C and 0.013 mbar for 1, 6, and 72 h.

Laboratory simulations of Mars-like conditions were performed in the Planetary Atmospheres and Surfaces Simulation Chamber (PASC) at the Centro de Astrobiologia (CAB) to understand UVR damage under martian surface conditions. The samples were pressed into 0.5 mm pellets and exposed to 74 h at room temperature (293 K), 7 mbar of CO_2, and UV irradiation from 200 to 400 nm. The UV flux measured at the sample position, obtained by integrating the spectral irradiance over the 200–400 nm wavelength range, was 2.3 × 1014 photons cm^2s^{-1}. This is comparable with three sols on the martian surface at equatorial latitudes (Mount and Rottman, 1983; Muñoz Caro et al., 2006).

3. Results

3.1. Sample descriptions

The three hydromagnesite microbialites used in this study represent a broad but distinct range of macroscopic and microscopic textures (Fig. 2).

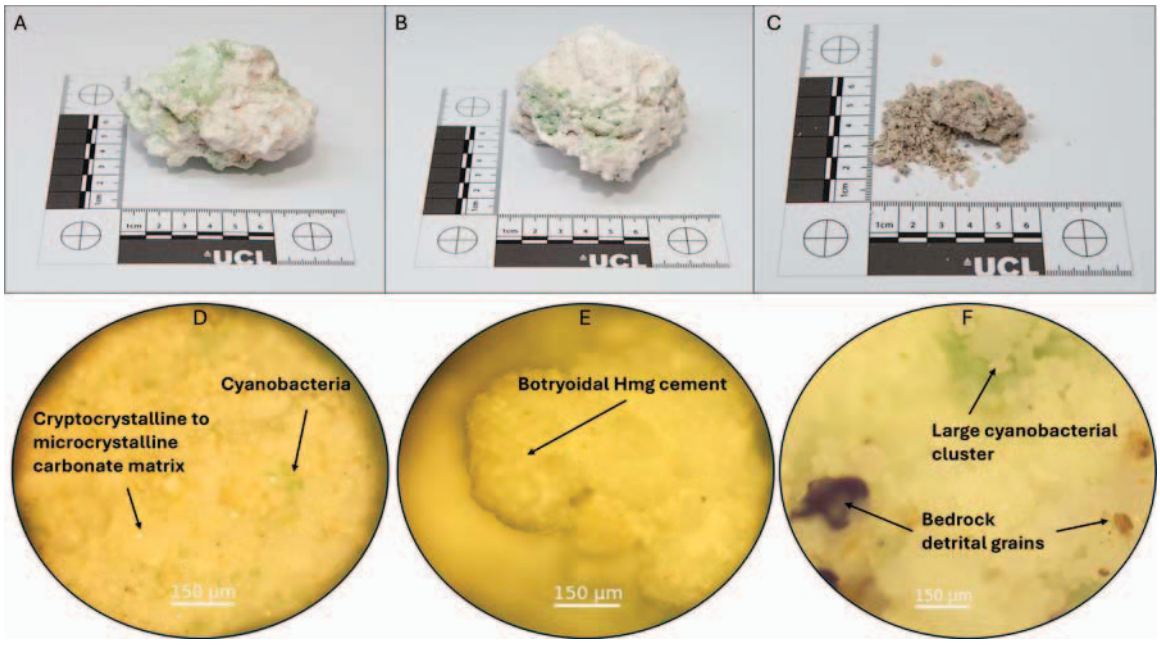

FIG. 2. Lake Salda microbialites referenced herein. **(A)** The Lower-Terrace Microbialite (LTM) and **(B)** the Mid-Terrace Microbialite (MTM) from the Eastern terrace system; **(C)** the Salda Gölü North Microbialite (SGNM), on the Northwestern flank of Lake Salda. **(D–F)** show the respective samples under 5X magnification using a binocular scope. The images highlight very fine crystal sizes, green cyanobacterial clusters, and botryoidal textures.

The LTM and MTM are intact and well cemented, whereas the freshly formed SGNM is friable and breaks into loose grains when it is handled (Fig. 2). All samples exhibit evidence of layered Mg carbonate precipitation in association with cyanobacterial EPS (Balci et al., 2020). The LTM and MTM have green cyanobacterial layers that overlie the white hydromagnesite surfaces, which indicates later-stage surface colonization. In contrast, the SGNM has discrete cyanobacterial clusters interspersed among its grains, with higher phyllosilicate content that gives it a darker color.

Microscopically, the LTM shows small cyanobacterial clusters and a cryptocrystalline to microcrystalline texture, while the MTM exhibits a botryoidal, well-cemented texture, not seen in the other microbialite samples. The SGNM contains abundant dark lithic clasts and poorly cemented carbonate grains, alongside dense green cyanobacterial clusters (Fig. 2). These textural differences indicate variation in cementation style, detrital input, and biological colonization (Russell et al., 1999; Zedef et al., 2000).

3.2. VisNIR analyses of the Lake Salda microbialites

Figure 3 represents VisNIR analyses of the LTM, MTM, and SGNM powdered subsamples, with their absorbtion features detailed in Table 2. Many OH (Clark et al., 1990; Whiting et al., 2004) and metal–OH (Al, Mg, Fe) absorptions feature in the 400–2500 nm range (Viscarra Rossel et al., 2009); this allows identification of contributory metal ions. The LTM and MTM spectra show absorptions at 1400 and 1958 nm due to lattice-bound OH and the bending and asymmetrical stretch combination band of interstitial H_2O (ν_2 + ν_3), respectively. Both bands are present in the SGNM, but the ν_2 + ν_3 H_2O band has combined with a smectite-related Al/Mg–OH vibration at 1911 nm, which has caused it to shift position to 1895 nm. The 959 and 1439 nm bands present in all spectra are assigned to smectite Fe^{3+}–O–H and Fe^{3+}/Mg–O–H overtones, respectively. A minor absorption in the SGNM at 1152 nm is tentatively assigned to the $3\nu_3$ CH_2 stretching mode (Stenberg et al., 2010).

Figure 4 shows VisNIR spectra of the LTM and MTM using a fiber optic illuminator attached to the RX Spec 700z VisNIR reflectance spectrometer. This enabled a ROI analysis to be executed on the complete sample, where we targeted white hydromagnesite carbonate and green cyanobacterial layers, well represented in both lower- and mid-terrace deposits. In this analysis, we show ROI spot 7a (white carbonate) + 1a (green microbial) of the LTM, and spot 1a (white carbonate) + 3b (green microbial) of the MTM as representatives of the respective layers. OH, Mg, and Fe^{3+} absorption bands are also observed with this technique and are featured in all fiber optic ROI and powdered VisNIR spectra. The most differentiating absorptions occur between 400 and 700 nm in the green microbial layers of both LTM and MTM, assigned to chlorophyll *a* (443 nm), carotenoids (498 nm), phycocyanin (629 nm), and chlorophyll *b* (687 nm).

3.3. FTIR analyses of the Lake Salda microbialites

Figure 5 shows FTIR spectra of the LTM, MTM, and SGNM, demonstrating the key spectral fingerprint region associated with carbonates, such as the C–O symmetric stretching (ν_1 1467 cm^{-1}), asymmetrical stretching (ν_3 1406 cm^{-1}), and bending modes (ν_2 750–800 cm^{-1}). Strong absorption features at 1118 cm^{-1} in all hydromagnesite microbialites are assigned to further C–O stretching of the carbonate mineralogy. The LTM and SGNM feature the ν_2 1643 cm^{-1} bending vibration

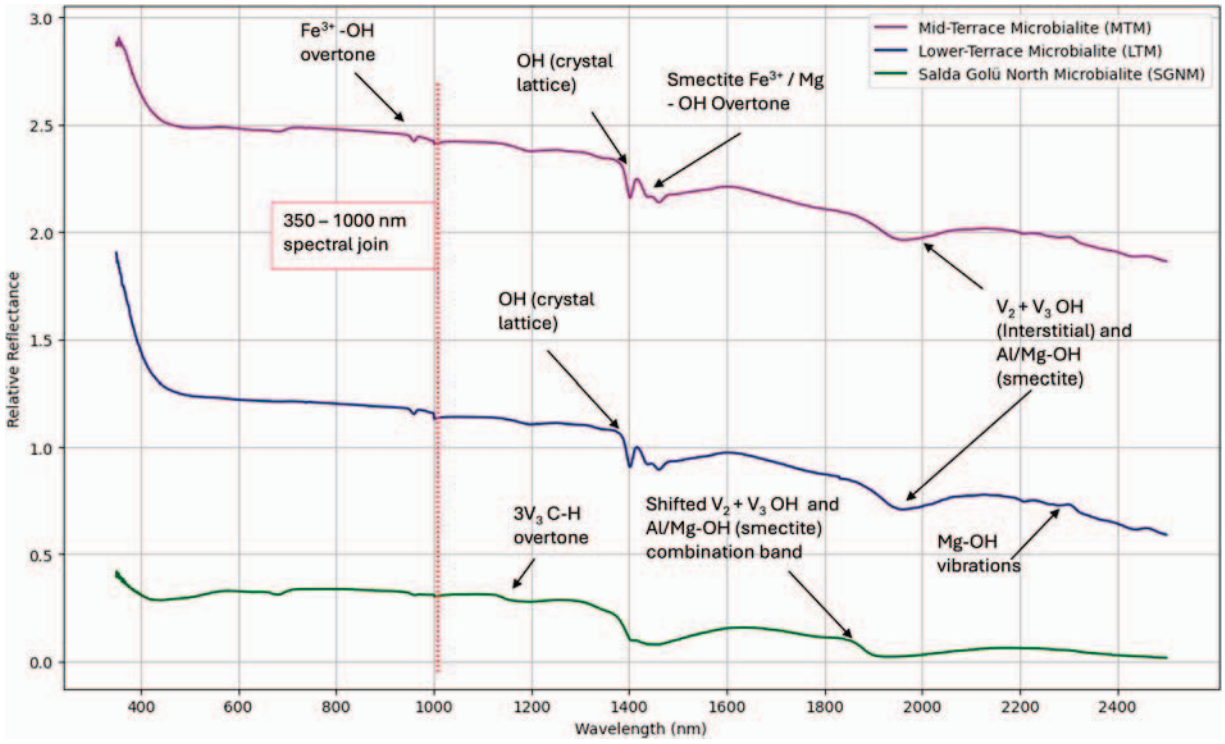

FIG. 3. VisNIR spectra of the LTM, MTM, and SGNM offset for comparison. All plots show the 1439 nm band assigned to Mg–O overtones, characteristic of hydromagnesite and Mg smectite. VisNIR, visible near-infrared.

Table 2. VisNIR Band Absorptions for the Lake Salda Microbialites

Peak position (cm^{-1})	*Band assignment*	*Reference*
443	Chlorophyll *a*	Dartnell and Patel, 2014
498	Carotenoids	Dartnell and Patel, 2014
629	Phycocyanin	Dartnell and Patel, 2014
687	Chlorophyll *b*	Dartnell and Patel, 2014
959	(Fe^{3+}–O–H) overtones	Clark et al., 1990
1152	$3\nu_3$ (CH_2)	Stenberg et al., 2010
1400	ν_1 (O–H) H_2O	Clark et al., 1990
1439	(Fe^{3+}/Mg–O–H) overtones	Whiting et al., 2004; Viscarra Rossel et al., 2009
1895	$\nu_2 + \nu_3$ (O–H) H_2O + (Al/Mg–O–H) combination	Clark et al., 1990; Viscarra Rossel et al., 2009
1911	(Al/Mg–O–H)	Clark et al., 1990; Viscarra Rossel et al., 2009
1958	$\nu_2 + \nu_3$ (O–H) H_2O combination	Clark et al., 1990; Whiting et al., 2004

VisNIR = visible near-infrared.

of H_2O, although it is noted that amide B (N–H bending) and amide I (C=O stretching) also occur at 1600–1700 cm^{-1} in organic-rich samples (Helm et al., 1991). Further absorption bands that form combined and convoluted peaks are assigned to aliphatic CH_2 ν_3 stretching (2923 cm^{-1}), interstitial OH stretching (3231, 3440 cm^{-1}), and coordinated Mg–OH stretching (3550, 3620 cm^{-1}). The MTM demonstrates similar coordinated OH and CO stretching and bending modes, with no organic features or interstitial H_2O absorptions, and thus presents a less intense profile. A complete list of absorbtion features are detailed in Table 3.

3.4. Lyophilization

Lyophilization enables the removal of interstitial pore water, thought to contribute to the broad, intense OH absorptions (2800–3600 cm^{-1}), which obscure underlying mineralogical and organic features. The samples were exposed to 0.013 mbar and −60°C over increasing timeframes. Table 4 reports the weights of the microbialite subsamples before and after lyophilization (referred to as the initial and sublimated weight) to show the loss of water (%) by sublimation. The sublimated weights for all three samples indicate a higher water content in the SGNM than in the MTM and LTM; they show a water loss of 22.5%, 0.5%, and 8.4%, respectively, after 1 h of exposure. Water loss increased during the 6 h exposure but decreased during 72 h, which suggests that samples are close to full sublimation between 1 and 6 h of lyophilization. We note that a decrease in water loss following a longer exposure time is a likely result of sample heterogeneity.

Figure 6 shows four FTIR spectra of the LTM, with the initial spectrum, taken before lyophilization, plotted against a 1, 6, and 72 h lyophilization cycle. A large intensity reduction is seen across all spectra following exposure, particularly in the broad OH region (2800–3600 cm^{-1}), H_2O ν_2 stretch at 1643 cm^{-1}, and the C–O ν_1 (1467 cm^{-1}), ν_2 (750–800 cm^{-1}), and ν_3 (1406 cm^{-1}) stretching and bending modes. The variability between peak shape and intensity is minimal after 6 and 72 h exposures; however, both these spectra show reduced C–O ν_1 (1467 cm^{-1}) and ν_3 (1406 cm^{-1}) intensity compared with the 1 h exposure, which demonstrates that further spectral alterations occur after 1 h of sublimation but are negligible past 6 h.

Figure 7 shows spectra of the initial SGNM against a 1, 6, and 72 h exposure. The initial spectrum shows very minor organic absorption features, particularly the aliphatic CH_2 ν_3 stretch (2923 cm^{-1}), deoxyribose C–O ν_1 stretch (1044 cm^{-1}), and the phosphate PO_2^- ν_3 stretching modes (1220 cm^{-1}); however, these are partially obscured and difficult to discern. In the 1, 6, and 72 h lyophilized samples, the relative intensity is drastically reduced across the entire spectra (Fig. 7). Little variation in peak height, shape, and intensity is observed between the 1, 6, and 72 h exposures, which overlap. When observing the 1 and 6 h lyophilized spectra alone, we see a notable relative intensity increase in the C–O ν_1 stretch (1044 cm^{-1}) and PO_2^- ν_3 stretching modes (1220 cm^{-1}), which become easier to discern following exposure. However, we see less organic preservation after 72 h, highlighted by reduced CH_2 ν_3 (2923 cm^{-1}) and PO_2^- ν_3 (1220 cm^{-1}) intensity (Fig. 8).

3.5. The Planetary Atmospheres and Surfaces Simulation Chamber

The LTM and SGNM microbialites were exposed to a simulated martian UV radiation environment via the PASC for 74 h (~3 martian days) and analyzed using FTIR spectroscopy. The microbialites were pressed into ~0.5 mm pellets and irradiated from a unidirectional source. These were powdered for ATR analysis, where we observed spectral characteristics consistent with UV penetration, concordant with the >500 μm UV attenuation of minerals documented by Carrier et al. (2019). Figure 8 shows a reduction in absorption intensity across both spectra after exposure, with significant reductions in O–H stretching modes at 1650 cm^{-1} and between 2800 and 3600 cm^{-1}. The exposed LTM spectra demonstrate a strong absorption for CO_2 not seen in any other spectra and unique to samples exposed via the PASC. The exposed SGNM demonstrates the destruction of the PO_2^- ν_3 phosphate backbone and ν_1 C–O deoxyribose organic absorptions, which were unique to this microbialite.

The exposed LTM spectrum shows a strong feature at 2358 cm^{-1} assigned to CO_2, not seen in spectra under Earth or sublimating conditions. Radiation exposure appears to destroy PO_2^- and C–O organics in the exposed SGNM spectrum. A reduction in intensity across the entire spectrum is observed in both samples following exposure.

4. Discussion

4.1. Visible and near-infrared spectroscopy

Visible and near-infrared spectroscopy is utilized on the martian surface by the Curiosity and Perseverance rovers

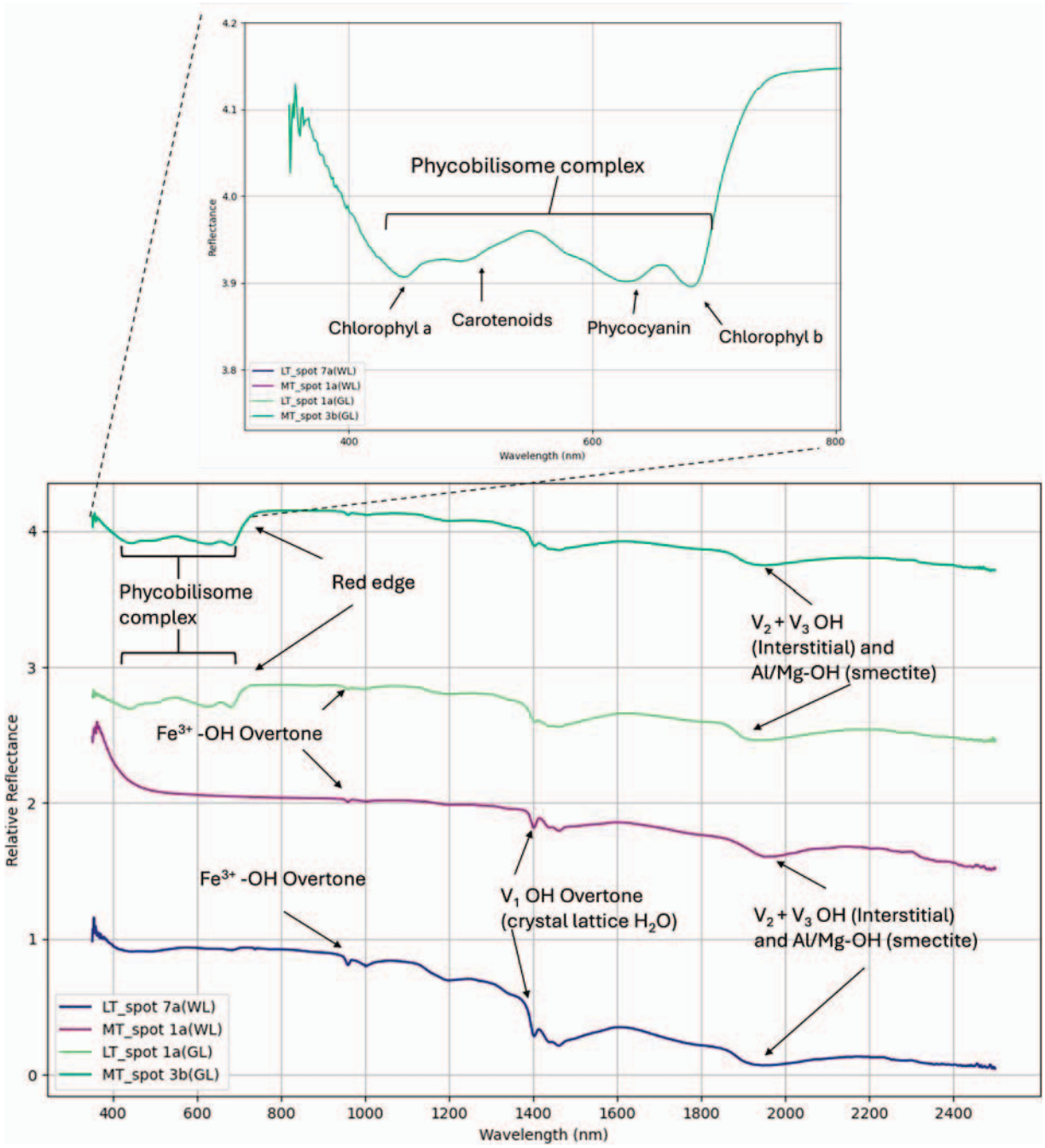

FIG. 4. VisNIR spectra of the LTM and MTM as seen using a fiber optic illuminator. Key absorption features pertaining to the phycobilisome light-harvesting complex (inlet shown) can be seen between 400 and 600 nm when the illuminator is directed toward the green cyanobacterial layer.

(Mahaffy et al., 2012; Farley et al., 2020) to infer the mineralogy of targets from distance. VisNIR analyses of the Lake Salda suite support the identification of metal ions, with distinct Al, Mg, and Fe^{3+} absorptions, which indicate the inclusion of phyllosilicates during hydromagnesite precipitation, incorporated within the microbialite matrix. These metal ions indicate the dominance of smectite clays at Lake Salda, likely composed of montmorillonite and nontronite (Clark et al., 1990; Madejová et al., 2017), which is consistent with recent observations (Garczynski et al., 2020). Aliphatic organics are difficult to observe in the NIR; however, the 1150 nm feature observed in the SGNM is tentatively assigned to the 3 ν_3 CH_2 stretching mode, due to the associated ν_3 fundamental vibration (2923 cm^{-1}) detected with FTIR analysis (Fig. 3). Organics in low quantities are therefore difficult to detect with VisNIR alone; a combination of spectral analyses is required to identify a greater number of organics, including those that could support a biosignature identification.

The fiber optic VisNIR illuminator was focused on regions of green biomass where absorptions that pertain to organics are differentiated from mineralogical absorptions,

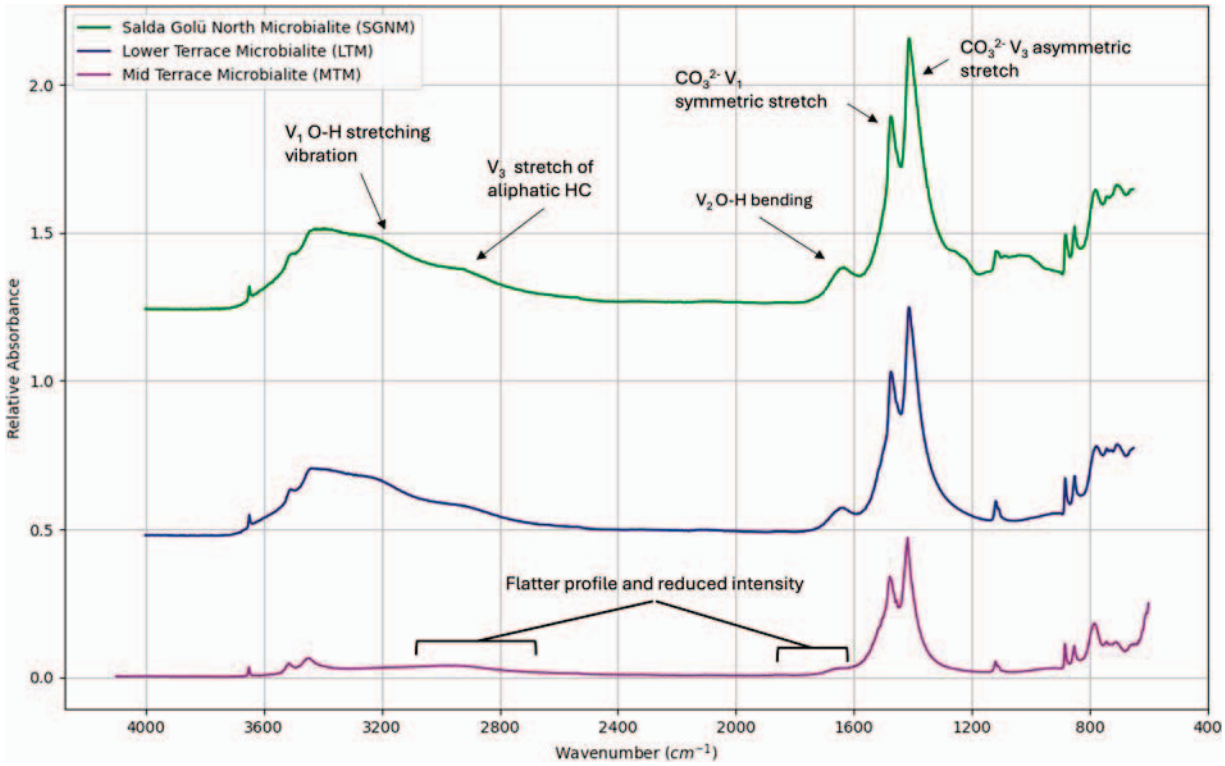

FIG. 5. FTIR spectra of the LTM, MTM, and SGNM, which are offset for comparison. Note the flatter overall profile of the MTM, particularly at 1650 cm^{-1} and 3231 cm^{-1}, 3440 cm^{-1} associated with OH absorptions. FTIR, Fourier transform infrared.

indicating which biosignatures are observable in the VisNIR wavelengths. Such spot measurements on ROIs suspected to contain biological material indeed showed intense organic absorption peaks in the 400–700 nm visible region (Fig. 4). The 443, 498, 629, and 687 nm absorptions are characteristic of the cyanobacterial pigment's chlorophyll *a*, carotenoids, phycocyanin, and chlorophyll *b*, respectively. These pigments conduct energy gathering and transfer within the cell. Chlorophyll *a*, *b*, and carotenoids are found in the thylakoid membrane, and phycocyanin comprises the phycobilisome light-harvesting complex (Dartnell et al., 2011). While these absorptions infer cellular constituents and form a pigment-related "red edge," a spectral biosignature in the search for life, these observations require a high volume of organic content. This is shown using a focused ∼5 mm sample area achieved with the fiber optic illuminator at ∼1.5 cm from the sample, which acts to reduce the spectral noise from undesired mineral-rich regions. As such, it would be difficult to observe biosignatures in the VisNIR range alone on the martian surface without the addition of other spectroscopic techniques like FTIR and Raman, or broader chemical, isotopic, textural, and mineralogical evidence gleaned from the sample or assemblage.

The SuperCam instrument onboard Perseverance offers four modes of spectroscopy: time-resolved Raman (TRR), time-resolved luminescence, laser-induced breakdown spectroscopy

Table 3. FTIR Band Absorptions for the Lake Salda Microbialites

Peak position (cm^{-1})	*Band assignment*	*Reference*
3620	ν_1 (Mg–OH)	Hare and Sorensen, 1992
3550	ν_1 (Mg–OH)	Du et al., 1993
3420	ν_1 (O–H) weak H bond	Boissiere et al., 2002; Bharmoria et al., 2012; Laurson et al., 2020
3250	ν_1 (O–H) strong H bond	Boissiere et al., 2002; Bharmoria et al., 2012; Laurson et al., 2020
2923	ν_3 (CH_2)	Helm et al., 1991; Preston et al., 2020
2885	ν_1 (CH_2)	Helm et al., 1991; Preston et al., 2020
1643	ν_2 (O–H)	Boissiere et al., 2002; Preston et al., 2020
1467	ν_1 (C–O) CO_3	Stuart, 2004; Gunasekaran et al., 2006
1406	ν_3 (C–O) CO_3	Stuart, 2004; Gunasekaran et al., 2006
1220	ν_3 (PO_2^-)	Brahms et al., 1974; Ahmad et al., 1996; Kelly et al., 2011
1118	ν_1 (C–O) CO_3	Stuart, 2004; Gunasekaran et al., 2006
1040	ν_1 (C–O) deoxyribose	Brahms et al., 1974; Ahmad et al., 1996; Kelly et al., 2011
750–800	ν_2 (C–O)CO_3	Stuart, 2004; Gunasekaran et al., 2006

FTIR = Fourier transform infrared.

Table 4. Initial and Sublimated Weight (g) for Lyophilized Subsamples and the Associated Water Loss (%) Following a 1, 6, and 72 h Exposure

	LTM	*MTM*	*SGNM*
Time exposed: 1 h			
Initial weight (g)	0.0945	0.0564	0.1875
Sublimated weight (g)	0.0865	0.0561	0.1454
Water loss (%)	8.466	0.532	22.453
Time exposed: 6 h			
Initial weight (g)	0.1132	0.124	0.1801
Sublimated weight (g)	0.103	0.123	0.1289
Water loss (%)	9.011	0.806	28.429
Time exposed: 72 h			
Initial weight (g)	0.1662	0.2613	0.2168
Sublimated weight (g)	0.1591	0.2602	0.1589
Water loss (%)	4.272	0.421	26.707

(LIBS), and visible (379–464 and 535–855 nm) and infrared (IRS 1.3–2.6 μm) spectroscopy (VISIR) (Clavé et al., 2023). Of all these, LIBS has been utilized most frequently (as of Sol 1100), with 203,000 shots compared with 148,000 for Raman and 8358 for IRS, due to the fine grain size of Jezero targets, where the Raman laser works best on larger and purer crystals (Cousin et al., 2024). The most recent observations by the IRS instrument in the Marginal Carbonate Unit describe three main signatures: a 1.9 μm hydration band, a 2.2 μm Si–OH band, and carbonate absorptions at 2.3 and 2.5 μm in association with some clays, thought to be Fe-phyllosilicates as indicated by a 2.39 μm band (Clavé et al., 2024). These absorptions are comparable with the Vis-NIR absorptions of the Lake Salda hydromagnesite microbialites (Figs. 3 and 4), showing that these deposits represent excellent mineralogical analogs for the Jezero Marginal Carbonate Unit.

4.2. FTIR spectroscopy

4.2.1. Textural influences on spectral interpretations. FTIR spectroscopy is advantageous when constraining fundamental mineralogical absorptions. The FTIR spectra of the Lower-, Mid-Terrace, and SGNM microbialites show variations in peak shape and intensity, which suggest various formation pathways or later alteration (Fig. 5). Interestingly, the MTM shows little organic or fundamental OH vibrational modes, likely due to the growth of a botryoidal hydromagnesite cement further observed through microscopy (Fig. 2). Botryoid morphologies have been reported close to organic matter in chert (Papineau et al., 2017) and malachite (Papineau, 2020), but also carbonates (Buongiorno et al., 2019; Papineau et al., 2021). Despite their spatial association with organics, the botryoidal cement that encapsulates the MTM removes all hydration features and appears to reduce the detection potential of organic biosignatures using FTIR spectroscopy. The destruction of features may not be attributed solely to the growth of botryoids, but rather to the subaerial processes (chemical/hydrological weathering and erosion) that form the hydromagnesite cements and botryoidal coatings observed in this study and documented herein (Braithwaite and Zedef, 1996, 1994; Russell et al., 1999). This observation demonstrates the sensitivity of microbially mediated deposits to weathering processes detrimental to structural and chemical traces of life, even across geologically short timespans ($\sim$14,000 years).

4.2.2. Key FTIR organic signatures. The detection of organics in hydromagnesite has implications for our ability to detect potential biosignatures in martian hydromagnesites at Jezero crater and at wider deposits from other locations on Mars. However, as demonstrated herein, they can be difficult to observe, even in terrestrial, geologically recent, and biologically mediated samples. FTIR spectroscopy has historically been used to assign band absorptions to bacterial cell

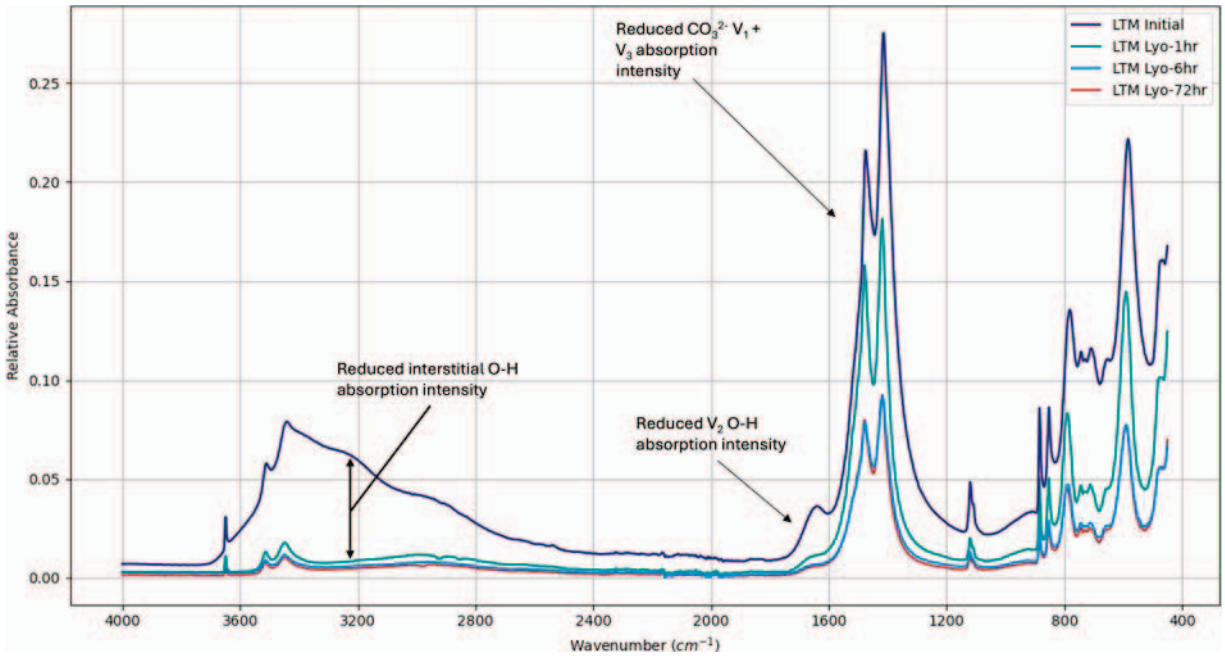

FIG. 6. FTIR spectra of the LTM before lyophilization and after 1, 6, and 72 h cycles. Intensity is significantly reduced following exposure across all regions.

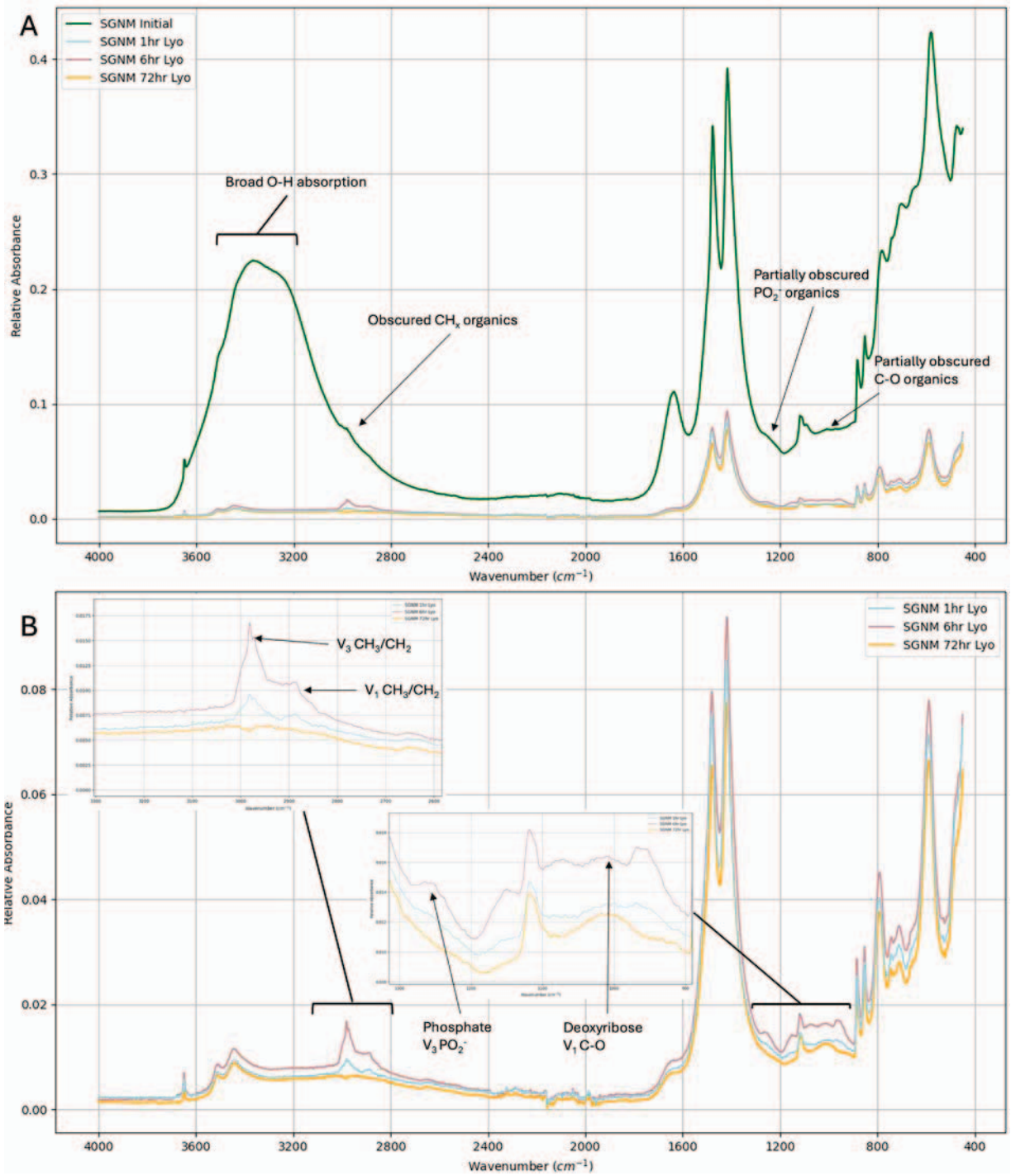

FIG. 7. **(A)** FTIR spectra of the SGNM before lyophilization and after 1, 6, and 72 h exposure. Intensity is significantly reduced following exposure across all regions. **(B)** FTIR spectra of the exposed SGNM only, which allow the identification of preserved organic features. Peaks associated with aliphatic hydrocarbons, PO_2^- backbone, and C–O deoxyribose are considered biosignatures and are easier to discern after 1 and 6 h lyophilization cycles.

components (Naumann et al., 1991; Preston et al., 2015, 2020, 2024). This includes aliphatic CH_2 ν_3 stretching vibrations (2923 cm^{-1}), which can be derived from various organic compounds such as fatty acids and lipids (Helm et al., 1991; Preston et al., 2014) and are documented in a variety of organic-bearing meteorites (Matrajt et al., 2004; Kebukawa et al., 2011; Okazaki et al., 2023). Identification of these organics in geologically relevant martian deposits may suggest more complex and potentially biologically useful organics were present. In Fig. 5, the 2923 cm^{-1} peak is tentatively assigned to CH_2 due to its relatively low intensity and broad nature, the likely result of strong OH absorptions in this spectral region, which can mask weak organic absorptions. In the preexposed spectrum, a more intense absorption

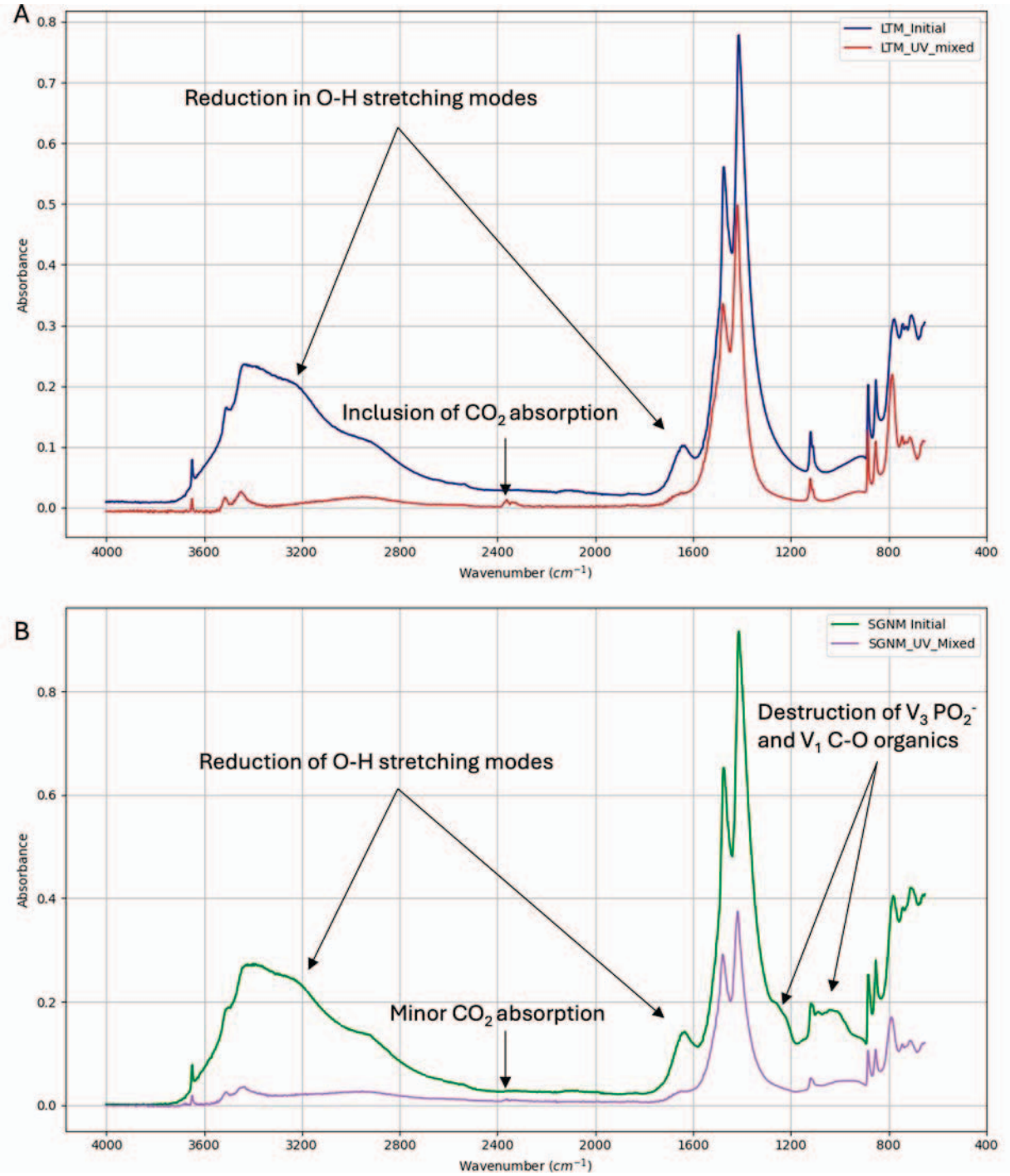

FIG. 8. FTIR spectra of the LTM **(A)** and SGNM **(B)** after exposure to simulated martian conditions for 74 h via the PASC. Following exposure, both samples exhibit reduced spectral intensities with the inclusion of a minor CO_2 absorption in the SGNM, which is more dominant in the LTM. PASC, Planetary Atmospheres and Surfaces Simulation Chamber.

peak is needed to confidently assign this as a biological aliphatic hydrocarbon attributed to the colonizing microbial mat.

Phosphate backbone (PO_2^-) stretching vibrations can occur around 1100–1230 cm^{-1}, and deoxyribose C–O stretching at 1000–1150 cm^{-1} (Brahms et al., 1974; Ahmad et al., 1996; Kelly et al., 2011); however, due to the degradation potential of these biomolecules, we expect a weak absorption peak. The intensity of the 1118 cm^{-1} feature, consistent across most hydromagnesite-bearing samples, implies this feature is a further C–O stretch related to the carbonate mineralogy. We do, however, see very minor absorptions at 1044 and 1220 cm^{-1} within the SGNM, not seen in any other microbialite spectra (Fig. 5). We assign these to deoxyribose C–O ν_1 stretching and the phosphate PO_2^- ν_3 stretching modes, respectively, due to the known organic content of the SGNM and the weak

nature of the features, as expected in biomolecules with high degradation potential. Nevertheless, these absorptions are difficult to discern in unexposed hydromagnesite deposits due to their relative intensity compared with more intense spectral features in the surrounding region, such as CO_3^{2-} stretching.

4.2.3. Intense FTIR OH absorptions. In FTIR spectroscopy, OH stretching absorptions between 3200 and 3620 cm^{-1} can overlap and become convoluted (Figs. 5, 7, and 8); the underlying absorptions can be broken into four separate OH bands through curve-fitting models documented in Boissiere et al. (2002), Bharmoria et al. (2012), Laurson et al. (2020), and references therein. These intense absorptions are largely attributed to the ~3250 and ~3420 cm^{-1} bands for strong and weakly H-bonded molecules, respectively (Bharmoria et al., 2012). Bands at ~3550 and ~3620 cm^{-1} are attributed to the coupling of OH asymmetrical stretching modes (Du et al., 1993) and OH stretching modes from coordinated water molecules, respectively (Hare and Sorensen, 1992), likely bound to the Mg ions present in hydromagnesite. Such intense OH combinations can influence the interpretation of other absorptions usually found within the 3200–3620 cm^{-1} region, such as N–H and aliphatic hydrocarbons, which are key absorptions in the search for biosignatures (Preston et al., 2020), the latter partially visible in Figs. 5–7. The removal of interfering OH is therefore integral for the accurate interpretation of organic features. In this study, the nondestructive removal of water, achieved through lyophilization, enabled us to reduce the absorption intensity pertaining to convoluted OH to help resolve the underlying absorptions between 2800 and 3620 cm^{-1}. This is likely to occur on the martian surface environment once samples are brought to the surface.

4.3. Exposure to simulated martian conditions

Various aspects of the martian surface environment are considered hostile for terrestrial life-forms and deleterious for the organic compounds they leave behind. We focused on two surface conditions that can interfere with spectral interpretations on the surface and in returned samples: (1) a rapidly sublimating environment, emulated through lyophilization; and (2) intense UV radiation under a CO_2-rich atmosphere, achieved using the PASC. We analyzed samples under these conditions with FTIR spectroscopy, which is sensitive to water, mineralogical, and organic fundamental vibrations.

4.3.1. Sublimation. To infer the spectroscopic behavior of the Jezero Marginal Carbonate Unit and wider surface deposits, we exposed the Lake Salda deposits to sublimating martian surface conditions through lyophilization. At Jezero crater, diurnal temperatures cycle between 190 and 270 K (−83.15°C and −3.15°C) (Zorzano et al., 2024), with a mean surface pressure of 7.5 Mbar (Savijärvi et al., 2023), compared with 1013.25 Mbar on Earth. Lyophilization (freeze-drying) is a technique commonly used in the food or pharmaceutical industry to stabilize material for storage or distribution (Adams, 2007). It involves drying through the low-temperature, low-pressure removal of water by ice sublimation (Dziki, 2020), and it has been shown to increase the long-term stability of biological material, such as liposome drug delivery systems (Chen et al., 2010) and mRNA vaccines (Muramatsu et al., 2022). In the food industry, De Torres et al. (2010) noted that lyophilization is less aggressive than oven-drying methods and enables better preservation of volatile and polyphenolic compounds. Lyophilization can also preserve the structural integrity of biological materials, such as tissue cellular structure (Png et al., 2008). Although protein structure may denature under lyophilization (Moorthy et al., 2015), the addition of stabilizing additives can overcome protein denaturation before and during freezing (Moussa et al., 2018).

Lyophilization may even offer protection for DNA molecules, as the stability of DNA is influenced by the residual water content of the containing sample (Sharma and Klibanov, 2007); therefore, the removal of sample water through lyophilization results in fewer degradation reactions. The later storage of freeze-dried samples at 4°C or below can prevent the accumulation of DNA damage (Zhang et al., 2017). These studies demonstrate the preservation potential of a low-pressure, low-temperature environment created during the lyophilization process.

By emulating martian surface conditions, we observed an intensity reduction across the entire FTIR spectrum for all samples, while preserving any organics incorporated in the deposit during 1, 6, and 72 h exposures, revealing well-defined organic features that relate to DNA and aliphatic hydrocarbons (Fig. 7). This is achieved through the reduction of hydromagnesite (CO_3) and OH band intensity following sublimation via lyophilization, which results in a relative increase in organic intensity due to the conservation of organic material under lyophilizing conditions. The process of removing residual water using this nondestructive technique serves to increase our ability to detect spectral biosignatures. Despite this, we do not detect CH_2 or PO_2^- biosignatures after the 72 h exposure, which may indicate degradation at these exposure lengths; however, we cannot rule out sample heterogeneity as a factor, given that organics are unevenly distributed throughout the sample. These findings imply that the sublimating martian surface environment may actually help conserve organic signatures preserved within certain geological materials; however, further work is needed to understand if extended exposure to sublimation can degrade biosignatures within carbonate rocks over time. Nonetheless, organics within rocks close to the surface may still be impacted by the effects of intense UV radiation.

4.3.2. Radiation environment. UV is considered the most destructive form of radiation for organic compounds (Baqué et al., 2022). Although the penetration depth is constrained between 0 and 1 mm in various deposits (Carrier et al., 2019), latitude, regolith composition and consolidation, atmospheric dust load, seasonal variations, and orbital position may all contribute to varying levels of UV penetration at the surface (Patel et al., 2002, 2004; Rontó et al., 2003; Gómez-Elvira et al., 2014). Furthermore, the UV destruction of parent organic molecules through the breaking of functional bonds can create radicals that further damage the parent molecule (Ehrenfreund et al., 2001; Carrier et al., 2019). Even molecules somewhat resistant to direct UV damage are subject to UV-mediated chemical reactions, which can reduce their concentrations (Benner et al., 2000; Poch et al., 2013). Such reactions create highly oxidizing environments that can reach a depth of 200 m

(Bullock et al., 1994; Zent, 1998). As such, it is important to understand the chemical and spectroscopical stability of hydromagnesite and the organic biosignatures within, which is poorly constrained under martian UV intensities; without it, accurate mineralogical, astrobiological, and broader environmental interpretations are difficult.

Figure 8 shows the LTM and SGNM before and after exposure to a simulated martian atmosphere and radiation environment via the PASC. Organic signatures that relate to complex DNA molecules are highly susceptible to UV degradation, demonstrated by the reduction in PO_2^- backbone and C–O deoxyribose absorptions in the SGNM following exposure. This indicates that UV radiation achieves substantial damage to organics over short time periods in hydromagnesite deposits, and this has implications for the interpretation of hydromagnesite deposits on the martian surface. Following exposure, the spectral intensity of both the LTM and SGNM is drastically reduced, similar to that seen under sublimating conditions but to a lesser extent. This further indicates that removing interstitial pore water through a simulated martian environment influences all mineralogical absorptions in hydromagnesites, due to the nature of weak and strong hydrogen bonding (Bharmoria et al., 2012). Exposure to 7 mbar of CO_2 at room temperature is sufficient to reduce O–H stretching vibrations at 1650 and 3200 - 3620 cm^{-1} without the subzero temperatures of the martian surface. An absorption at 2358 cm^{-1} assigned to CO_2, unique to the PASC-exposed spectra, may be incorporated from the induced CO_2-rich atmosphere. In the presence of CO_2, hydromagnesite can become a carbon sink, although CO_2 sequestration is often initiated through mineral carbonation (Power et al., 2009; Turvey et al., 2018; Zhang et al., 2020), forming stable Mg carbonates that would not contribute to the spectral detection of CO_2, as seen in Fig. 8, which suggests an alternative origin. CO_2 can also result from the photolysis of organic matter by UV radiation (Moran and Zepp, 1997; Brandt et al., 2009; McLeod et al., 2021, and references therein). Photolysis can initiate CO_2 outgassing, which becomes trapped in the mineral interstitial pore space and is detectable using FTIR spectroscopy. Given the biotic nature of the Lake Salda deposits and the spectral identification of organic molecules, CO_2 trapping via photolysis is plausible; however, we note that atmospheric CO_2 can occur as an artifact during spectroscopy and cannot be ruled out from this study. A very minor CO_2 absorption can be seen in the SGNM-exposed spectrum, despite the higher volume of organic content; therefore, CO_2 loss cannot be accurately quantified using spectral intensity alone, as not all CO_2 from organic matter photolysis becomes trapped in the sample and visible through FTIR spectroscopy. Nevertheless, the influence of UV radiation on spectral features is evident and should be noted for the accurate interpretation of martian hydromagnesite deposits when using spectroscopic techniques.

4.4. Consequences for Mars rover and sample return missions

4.4.1. Sampling from shallow depths (<10 cm). Given the dehydration of various phases observed on the martian surface, including perchlorates (Martín-Torres et al., 2015) and sulfates (Schopf et al., 2012), it is likely that surficial hydromagnesite deposits have undergone varying degrees of sublimation of interstitial water. This may increase our ability to detect organics using vibrational spectroscopy as demonstrated herein, although the surface environment is not conducive to biosignature preservation. Although samples collected up to a depth of 78 mm by the Perseverance rover may evade damaging UV radiation (Carrier et al., 2019), the top 5–10 cm of outcrops >300 Ma experience the deleterious effects of intense ionizing radiation, which may extend to 2 m at lesser intensities (Pavlov et al., 2012).

This has implications for the spectral interpretation of minerals by SuperCam (1.3–2.6 μm) onboard the Perseverance rover, which analyzes surface deposits to help collect samples from the shallow subsurface ≤78 mm. SuperCam surface spectra may show fewer hydration features and broad-spectrum low absorption intensities, both of which may increase with sample depth. Complex organics will be difficult to observe at these depths due to UV and cosmic radiation intensities; however, simpler organics that result from photolysis may be detectable, and hydromagnesite spectra with CO_2 overtones across 1.3–2.6 μm would be a good indicator of this process, as their fundamental vibrations are detected using FTIR spectroscopy (Fig. 8).

The behavior of hydromagnesite in this study is applicable to interpretations of the Jezero Marginal Unit among other martian carbonate deposits and further suggests that the spectral interpretations of broader hydrated mineral phases, such as phyllosilicates, may be impacted by the sublimation of interstitial pore water. This should be considered for upcoming missions such as Rosalind Franklin, which is proposed to investigate the phyllosilicate-dominant Oxia Planum. Interpretations for this mission would be benefited by further work on the spectral behavior of phyllosilicate-rich deposits that undergo sublimation at different timescales.

5. Conclusion

Hydromagnesite deposition at Lake Salda forms a useful terrestrial analog for the Marginal Carbonate Unit at Jezero crater. Lake Salda hydromagnesite is predominately deposited through the reworking of hydromagnesite microbialites, produced by cyanobacterial mats. While alternative origins for the Jezero Marginal Unit have been proposed, the Lake Salda system shows that biologically mediated deposition cannot be ruled out. This study sought to understand the nature of organic preservation in hydromagnesite via FTIR and VisNIR spectroscopy and to assess mineralogical and organic biosignature spectral alterations following exposure to simulated martian conditions.

Initial FTIR characterization of the LTM and SGNM conforms to reference hydromagnesite spectra but with intense absorptions associated with interstitial OH stretching (3231, 3440 cm^{-1}) and coordinated Mg–OH stretching (3550, 3620 cm^{-1}). Among these absorptions, the SGNM exhibits minor CH_2 ν_3 stretching (2923 cm^{-1}), deoxyribose C–O ν_1 stretching (1044 cm^{-1}), and phosphate PO_2^- ν_3 stretching modes (1220 cm^{-1}); this demonstrates the potential of hydromagnesite to preserve organic biomass. The MTM is the only microbialite not to feature OH and organic absorptions, a likely result of botryoidal cement formation through subaerial weathering, shown to reduce OH retention and organic signature preservation in the study samples. This suggests that carbonate alteration can affect spectral signatures and their

interpretation, particularly in the context of paleoenvironmental reconstruction and the search for organic biosignatures.

Organic matter can be sensitive to changes in the moisture content of host rocks. Under the sublimating conditions of the martian surface, samples may experience rapid sublimation when the weight of overlying rock is reduced during exhumation, such as may occur for samples collected from depth by the Rosalind Franklin rover. In this study, we simulated rapid sublimation through lyophilization, following which the spectral intensity of the exposed LTM, MTM, and SGNM samples was drastically reduced after just 1 h, which indicates the influence that interstitial water has on bond vibrational intensities, attributed to the reduction of strong and weak hydrogen bonding. Despite this, the organic content of the SGNM was conserved throughout the sublimation process, enabling an increase in the relative intensity of organic signatures, which became more apparent after exposure. These results indicate that hydromagnesites, alongside phyllosilicates and other water-binding sediments, may be easier to interpret spectrally when sublimated if searching for organic biosignatures, significant for future rover missions that are planned to sample from depths where the sublimation of volatiles during core exhumation is likely, such as Rosalind Franklin. VisNIR spectroscopy reveals contributory metal ions in metal–OH bonds and reveals clay mineral inclusions associated with vermiculite and montmorillonite. Organics, however, are difficult to observe in the NIR, with the SGNM 1150 nm feature tentatively assigned to the 3 ν_3 CH_2 stretching mode. We do identify constituents of the phycobilisome light-harvesting complex in the visible wavelengths (400–700 nm), although this detection requires a target with high organic content and a high signal-to-noise instrument, demonstrated in this study using a fiber optic illuminator <1.5 cm from the sample target area. This implies that visible-wavelength organic detections may be difficult on the martian surface if spectra are taken from distances >1 m, typical of rover instruments like SuperCam, PanCam, or Enfys, considering targets are exposed to deleterious surface conditions for long time periods.

A reduction in spectral intensity is observed in the PASC-exposed samples, attributed to the removal of sample water under the 7 mbar simulation conditions. In the SGNM sample, features considered as organic biosignatures, the CH_2 ν_3 stretching (2923 cm^{-1}), deoxyribose C–O ν_1 stretching (1044 cm^{-1}), and phosphate PO_2^- ν_3 stretching modes (1220 cm^{-1}), are greatly reduced by radiation exposure, which induces the photolysis of organic content over 74 h. The photolysis of complex organics in Lake Salda microbialites may contribute to the spectral detection of CO_2, although the exact origin of this feature is unclear. The radiation-induced spectral characteristics seen in this analog study provide groundwork for improving the interpretations of martian samples.

Given these results, we provide consequences for Mars rover and sample return missions, detailed above, and follow this with suggested protocols to aid spectral interpretation of martian samples going forward.

5.1. Protocols to improve spectral interpretations

A significant finding in this study is the increased spectral absorption intensity with increasing sample hydration. Sublimation of hydrated subsurface samples will occur rapidly at the martian surface, and spectral interpretations will differ depending on where the samples originated and for how long they were exposed at the surface. Despite changes in spectral intensity following sublimation, organic signatures are preserved and become more detectable relative to the reduced O–H and mineral absorption intensity, which decreases as samples are sublimated. While we saw intensity reductions in the PASC experiments, likely due to partial sublimation, these samples had been exposed to UV radiation, which resulted in degradation of organic signatures. Given this, we provide suggestions on sampling protocols to enable accurate spectral interpretations when on the martian surface:

1. Samples with pores (carbonates) or micropores (phyllosilicates) can uptake and hold interstitial water. Those beneath the subsurface ($\sim$0.2–2 m) may contain small volumes of interstitial water that can overprint less intense organic signatures. Sublimated samples would produce clearer spectra for biosignature interpretations; therefore, allowing sublimation within the Analytical Laboratory Drawer (ALD) unit would improve the interpretation of organics when using spectroscopic techniques. This is likely to occur in <1 h at martian surface pressures, given the behavior of the samples under simulated conditions within this study.
2. Noting spectral absorption changes between borehole readings (MaMiss) and ALD (MicroMega) measurements can provide information on volatile composition and loss. Spectral changes in the key O–H regions documented herein should therefore be expected and accounted for.
3. The UV environment is shown to be particularly damaging to organics in relatively short timeframes (≤74 h). Samples exhumed to the surface should be shielded from UV radiation instantly, or as soon as feasible. Moving samples inside the rover's ALD (Rosalind Franklin) or sealing them inside sample tubes (Perseverance) should provide UV protection and thermal stability and prevent terrestrial atmospheric contamination when returned via MSR (Moeller et al., 2021).
4. Any samples returned to Earth from future sample return missions could be subsampled, with smaller volumes exposed to sublimating conditions to reduce the spectral noise associated with volatiles, especially if the identification of organics is the primary focus.

Acknowledgments

The authors would like to thank Science and Technology Facilities Council (STFC) for the support of C.J.B. via a studentship and L.J.P. via the consolidated grant ST/W001004/1. C.J.B. acknowledges the University of Westminster for the use of the lyophilizer and VisNIR instruments.

Author Disclosure Statement

No competing financial interests exist.

Funding Information

The PASC experiments were supported by project PID2022-140180OB-C22 of the Spanish Ministry of Science and

Innovation, and we thank S. Galvez-Martínez for his technical support during the experiments in the PASC simulation chamber.

References

Adams G. The principles of freeze-drying. In: *Cryopreservation and Freeze Drying Protocols*. Springer: New York; 2007; pp. 15–38.

Ahmad R, Naoui M, Neault JF, et al. An FTIR spectroscopic study of calf-thymus DNA complexation with Al(III) and Ga (III) cations. *J Biomol Struct Dyn* 1996;13(5):795–802; doi: 10.1080/07391102.1996.10508892

Allwood AC, Walter MR, Kamber BS, et al. Stromatolite reef from the early Archaean era of Australia. *Nature* 2006; 441(7094):714–718; doi: 10.1038/nature04764

Balci N, Gunes Y, Kaiser J, et al. Biotic and abiotic imprints on Mg-Rich stromatolites: Lessons from Lake Salda, SW Turkey. *Geomicrobiol J* 2020;37(5):401–425; doi: 10.1080/01490451.2019.1710784

Baqué M, Backhaus T, Meeßen J, et al. Biosignature stability in space enables their use for life detection on Mars. *Sci Adv* 2022;8(36):eabn7412; doi: 10.1126/sciadv.abn7412

Benner SA, Devine KG, Matveeva LN, et al. The missing organic molecules on Mars. *Proc Natl Acad Sci U S A* 2000; 97(6):2425–2430; doi: 10.1073/pnas.040539497

Benning LG, Phoenix VR, Yee N, et al. The dynamics of cyanobacterial silicification: An infrared micro-spectroscopic investigation. *Geochim Cosmochim Acta* 2004;68(4):743–757; doi: 10.1016/S0016-7037(03)00488-5

Bharmoria P, Gupta H, Mohandas VP, et al. Temperature invariance of NaCl solubility in water: Inferences from salt–water cluster behavior of NaCl, KCl, and NH_4CL. *J Phys Chem B* 2012;116(38):11712–11719; doi: 10.1021/jp307261g

Boissiere C, Brubach JB, Mermet A, et al. Water confined in lamellar structures of AOT surfactants: An infrared investigation. *J Phys Chem B* 2002;106(5):1032–1035; doi: 10.1021/jp012724i

Bontognali TRR, Vasconcelos C, Warthmann RJ, et al. Dolomite formation within microbial mats in the coastal Sabkha of Abu Dhabi (United Arab Emirates). *Sedimentology* 2010; 57(3):824–844; doi: 10.1111/j.1365-3091.2009.01121.x

Bradbury HJ, Halloran KH, Lin CY, et al. Calcium isotope fractionation during microbially induced carbonate mineral precipitation. *Geochim Cosmochim Acta* 2020;277:37–51; doi: 10.1016/j.gca.2020.03.014

Brahms S, Brahms J, Pilet J. Infrared studies on the backbone conformation of nucleic acids. *Isr J Chem* 1974;12(1–2): 153–163; doi: 10.1002/ijch.197400015

Braissant O, Cailleau G, Dupraz C, et al. Bacterially induced mineralization of calcium carbonate in terrestrial environments: The role of exopolysaccharides and amino acids. *J Sedimentary Res* 2003;73(3):485–490; doi: 10.1306/111302730485

Braithwaite CJR, Zedef V. Hydromagnesite stromatolites and sediments in an alkaline lake, Salda Gölü, Turkey. *J Sedimentary Res* 1996;66(5):991–1002; doi: 10.1306/D426845F-2B26-11D7-8648000102C1865D

Braithwaite CJR, Zedef V. Living hydromagnesite stromatolites from Turkey. *Sediment Geol* 1994;92(1–2):1–5; doi: 10.1016/0037-0738(94)90051-5

Brandt LA, Bohnet C, King JY. Photochemically induced carbon dioxide production as a mechanism for carbon loss from plant litter in arid ecosystems. *J Geophys Res* 2009;114(G2); doi: 10.1029/2008JG000772

Bullock MA, Stoker CR, McKay CP, et al. A coupled soil-atmosphere model of H_2O_2 on Mars. *Icarus* 1994;107(1): 142–154; doi: 10.1006/icar.1994.1012

Buongiorno J, Gomez FJ, Fike DA, et al. Mineralized microbialites as archives of environmental evolution, Laguna Negra, Catamarca Province, Argentina. *Geobiology* 2019;17(2):199–222; doi: 10.1111/gbi.12327

Carrier BL, Abbey WH, Beegle LW, et al. Attenuation of ultraviolet radiation in rocks and minerals: Implications for Mars science. *JGR Planets* 2019;124(10):2599–2612; doi: 10.1029/2018JE005758

Chen C, Han D, Cai C, et al. An overview of liposome lyophilization and its future potential. *J Control Release* 2010;142(3): 299–311; doi: 10.1016/j.jconrel.2009.10.024

Clark RN, King TVV, Klejwa M, et al. High spectral resolution reflectance spectroscopy of minerals. *J Geophys Res* 1990; 95(B8):12653–12680; doi: 10.1029/JB095iB08p12653

Clavé E, Beck P, Beyssac O, et al. New constraints on the "marginal carbonates" from *in situ* observations with Supercam, Mars2020. *Europlanet Science Congress* 2024;17:EPSC2024-255; doi: 10.5194/epsc2024-255

Clavé E, Benzerara K, Meslin P-Y, et al. Carbonate detection with Supercam in igneous rocks on the floor of Jezero Crater, Mars. *JGR Planets* 2023;128(6):e2022JE007463; doi: 10.1029/2022JE007463

Cousin A, Wiens RC, Clegg S, et al. The Supercam instrument onboard Perseverance: Overview of efforts compiled for Mars x conference. In: *Tenth International Conference on Mars*. Lunar and Planetary Institute: Houston, 2024; abstract 3169.

Cousins CR, Mikhail S, Foucher F, et al. Metamorphic evolution of carbonate-hosted microbial biosignatures. *Geochem Persp Let* 2020;12(12):40–45; doi: 10.7185/geochemlet.2002

Dartnell LR, Desorgher L, Ward JM, et al. Martian sub-surface ionising radiation: Biosignatures and geology. *Biogeosciences* 2007b;4(4):545–558; doi: 10.5194/bg-4-545-2007

Dartnell LR, Desorgher L, Ward JM, et al. Modelling the surface and subsurface Martian radiation environment: Implications for astrobiology. *Geophys Res Lett* 2007a;34(2); doi: 10.1029/2006GL027494

Dartnell LR, Patel MR. Degradation of microbial fluorescence biosignatures by solar ultraviolet radiation on Mars. *Int J Astrobiol* 2014;13(2):112–123; doi: 10.1017/S1473550413000335

Dartnell LR, Storrie-Lombardi MC, Mullineaux CW, et al. Degradation of cyanobacterial biosignatures by ionizing radiation. *Astrobiology* 2011;11(10):997–1016; doi: 10.1089/ast.2011.0663

Davraz A, Sener E, Sener S. Evaluation of climate and human effects on the hydrology and water quality of Burdur Lake, Turkey. *J Afr Earth Sci* 2019;158:103569; doi: 10.1016/j.jafrearsci.2019.103569

De Torres C, Díaz-Maroto MC, Hermosín-Gutiérrez I, et al. Effect of freeze-drying and oven-drying on volatiles and phenolics composition of grape skin. *Anal Chim Acta* 2010; 660(1–2):177–182; doi: 10.1016/j.aca.2009.10.005

Direito SOL, Marees A, Röling WFM. Sensitive life detection strategies for low-biomass environments: Optimizing extraction of nucleic acids adsorbing to terrestrial and Mars analogue minerals. *FEMS Microbiol Ecol* 2012;81(1):111–123; doi: 10.1111/j.1574-6941.2012.01325.x

Du Q, Superfine R, Freysz E, et al. Vibrational spectroscopy of water at the vapor/water interface. *Phys Rev Lett* 1993; 70(15):2313–2316; doi: 10.1103/PhysRevLett.70.2313

Dupraz C, Reid RP, Braissant O, et al. Processes of carbonate precipitation in modern microbial mats. *Earth Sci Rev* 2009; 96(3):141–162; doi: 10.1016/j.earscirev.2008.10.005

Dupraz C, Visscher PT, Baumgartner LK, et al. Microbe–mineral interactions: Early carbonate precipitation in a hypersaline lake (Eleuthera Island, Bahamas). *Sedimentology* 2004; 51(4):745–765; doi: 10.1111/j.1365-3091.2004.00649.x

Dupraz C, Visscher PT. Microbial lithification in marine stromatolites and hypersaline mats. *Trends Microbiol* 2005; 13(9):429–438; doi: 10.1016/j.tim.2005.07.008

Dziki D. Recent trends in pretreatment of food before freeze-drying. *Processes* 2020;8(12):1661; doi: 10.3390/pr8121661

Ehrenfreund P, Bernstein MP, Dworkin JP, et al. The photostability of amino acids in space. *Astrophys J* 2001;550(1): L95–L99; doi: 10.1086/319491

Farley KA, Williford KH, Stack KM, et al. Mars 2020 mission overview. *Space Sci Rev* 2020;216(8):142; doi: 10.1007/s11214-020-00762-y

Garczynski B, Horgan B, Kah L, et al. Expected results of carbonate investigations by the Perseverance rover in Jezero Crater: Lessons from a fluviolacustrine analog at Lake Salda, Turkey. *Planet Space Sci* 2021;67(1):28–45.

Garczynski B, Horgan B, Kah L, et al. Searching for potential biosignatures in Jezero Crater, Mars with the NASA Perseverance rover: Lessons from a fluviolacustrine analog at Lake Salda, Turkey. In: *75th Geological Congress of Turkey with international participation 2023; April 10–14, 2022*, Ankara, Turkey; 2023.

Garczynski BJ, Horgan B, Kah LC, et al. Investigating the origin of carbonate deposits in Jezero Crater: Mineralogy of a fluviolacustrine analog at Lake Salda, Turkey. In: *51st Lunar and Planetary Science Conference*. Lunar and Planetary Institute: Houston, 2020; abstract 2128.

Garczynski BJ, Horgan B, Kah LC, et al. Searching for potential biosignatures in Jezero Crater with Mars 2020—A spectral investigation of terrestrial lacustrine carbonate analogs. In: *Ninth International Conference on Mars*. Lunar and Planetary Institute: Houston, 2019; abstract 6302.

Gil-Lozano C, Fairén AG, Munõz-Iglesias V, et al. Constraining the preservation of organic compounds in Mars analog nontronites after exposure to acid and alkaline fluids. *Sci Rep* 2020;10(1):15097; doi: 10.1038/s41598-020-71657-9

Gómez-Elvira J, Armiens C, Carrasco I, et al. Curiosity's rover environmental monitoring station: Overview of the first 100 sols. *J Geophys Res Planets* 2014;119(7):1680–1688; doi: 10.1002/2013JE004576

Grady MM. Astrobiology of the terrestrial planets, with emphasis on Mars. In: *Complete Course in Astrobiology*. (Horneck G, Rettberg P. eds.) John Wiley: Chichester, UK, 2007; pp. 203–222.

Gunasekaran S, Anbalagan G, Pandi S. Raman and infrared spectra of carbonates of calcite structure. *J Raman Spectroscopy* 2006;37(9):892–899; doi: 10.1002/jrs.1518

Gunes Y, Baldes MJ, Gong J, et al. Morphospace, composition and texture of Lake Salda microbialites. In: *EGU General Assembly Conference Abstracts*. European Geosciences Union: Vienna, Austria, 2022; (Technical Report EGU22-395); doi: 10.5194/egusphere-egu22-395

Gunes Y, Sekerci F, Avcı B, et al. Morphological and microbial diversity of hydromagnesite microbialites in Lake Salda, a Mars analog alkaline Lake. *bioRxiv* 2023; doi: 10.1101/2023.09.06.556485

Hare DE, Sorensen CM. Interoscillator coupling effects on the OH stretching band of liquid water. *J Chem Phys* 1992;96(1): 13–22; doi: 10.1063/1.462852

Helm D, Labischinski H, Schallehn G, et al. Classification and identification of bacteria by Fourier-transform infrared spectroscopy. *J Gen Microbiol* 1991;137(1):69–79; doi: 10.1099/00221287-137-1-69

Kaiser J, Ön B, Arz HW, et al. Sedimentary lipid biomarkers in the magnesium rich and highly alkaline Lake Salda (southwestern Anatolia). *J Limnol* 2016;75(3); doi: 10.4081/jlimnol.2016.1337

Kasper JC, Winter G, Friess W. Recent advances and further challenges in lyophilization. *Eur J Pharm Biopharm* 2013; 85(2):162–169; doi: 10.1016/j.ejpb.2013.05.019

Kawaguchi T, Decho AW. A laboratory investigation of cyanobacterial extracellular polymeric secretions (EPS) in influencing $CaCO_3$ polymorphism. *J Cryst Growth* 2002b;240(1–2): 230–235; doi: 10.1016/S0022-0248(02)00918-1

Kawaguchi T, Decho AW. Isolation and biochemical characterization of extracellular polymeric secretions (EPS) from modern soft marine stromatolites (Bahamas) and its inhibitory effect on $CaCO_3$ precipitation. *Prep Biochem Biotechnol* 2002a;32(1):51–63; doi: 10.1081/PB-120013161

Kazanci N, Girgin S, Dügel M. On the limnology of Salda Lake, a large and deep soda Lake in Southwestern Turkey: Future management proposals. *Aquatic Conservation* 2004; 14(2):151–162; doi: 10.1002/aqc.609

Kebukawa Y, Alexander C, Cody GD. Compositional diversity in insoluble organic matter in type 1, 2 and 3 chondrites as detected by infrared spectroscopy. *Geochim Cosmochim Acta* 2011;75(12):3530–3541; doi: 10.1016/j.gca.2011.03.037

Kelly JG, Najand GM, Martin FL. Characterisation of DNA methylation status using spectroscopy (mid-IR versus Raman) with multivariate analysis. *J Biophotonics* 2011;4(5): 345–354; doi: 10.1002/jbio.201000085

Laurson P, Raudsepp P, Kaldmäe H, et al. The deconvolution of FTIR-ATR spectra to five gaussians for detection of small changes in plant–water clusters. *AIP Advances* 2020;10(8); doi: 10.1063/5.0011700

Madejová J, Gates WP, Petit S. IR spectra of clay minerals. *Dev Clay Sci* 2017;8:107–149; doi: 10.1016/B978-0-08-100355-8.00005-9

Mahaffy PR, Webster CR, Cabane M, et al. The Sample Analysis at Mars investigation and instrument suite. *Space Sci Rev* 2012;170(1–4):401–478; doi: 10.1007/s11214-012-9879-z

Margulis L, Mazur P, Barghoorn ES, et al. The Viking mission: Implications for life on mars. *J Mol Evol* 1979;14(1–3): 223–232; doi: 10.1007/BF01732380

Martín-Torres J, Zorzano M-P, Valentín-Serrano P, et al. Transient liquid water and water activity at Gale Crater on Mars. *Nature Geosci* 2015;8(5):357–361; doi: 10.1038/ngeo2412

Matrajt G, Borg J, Raynal PI, et al. FTIR and Raman analyses of the Tagish Lake meteorite: Relationship with the aliphatic hydrocarbons observed in the diffuse interstellar medium. *A&A* 2004;416(3):983–990; doi: 10.1051/0004-6361:20034526

McLeod AR, Brand T, Campbell CN, et al. Ultraviolet radiation drives emission of climate-relevant gases from marine

phytoplankton. *JGR Biogeosciences* 2021;126(9):e2021JG006345; doi: 10.1029/2021JG006345

Melim LA, Northup DE, Boston PJ, et al. Preservation of fossil microbes and biofilm in cave pool carbonates and comparison to other microbial carbonate environments. *Palaios* 2016; 31(4):177–189; doi: 10.2110/palo.2015.033

Moeller RC, Jandura L, Rosette K, et al. The Sampling and Caching Subsystem (SCS) for the scientific exploration of Jezero Crater by the mars 2020 perseverance rover. *Space Sci Rev* 2021;217(1):5; doi: 10.1007/s11214-020-00783-7

Moorthy BS, Iyer LK, Topp EM, et al. Characterizing protein structure, dynamics and conformation in lyophilized solids. *Curr Pharm Des* 2015;21(40):5845–5853; doi: 10.2174/1381612821666151008150735

Moran MA, Zepp RG. Role of photoreactions in the formation of biologically labile compounds from dissolved organic matter. *Limnology & Oceanography* 1997;42(6):1307–1316; doi: 10.4319/lo.1997.42.6.1307

Mount GH, Rottman GJ. The solar absolute spectral irradiance 1150–3173 Å: May 17, 1982. *J Geophys Res* 1983;88(C9): 5403–5410; doi: 10.1029/JC088iC09p05403

Moussa EM, Singh SK, Kimmel M, et al. Probing the conformation of an IgG1 monoclonal antibody in lyophilized solids using solid-state hydrogen–deuterium exchange with mass spectrometric analysis (ssHDX-MS). *Mol Pharm* 2018;15(2): 356–368; doi: 10.1021/acs.molpharmaceut.7b00696

Muñoz Caro GM, Mateo-Martí E, Martínez-Frías J. Near-UV transmittance of basalt dust as an analog of the martian regolith: Implications for sensor calibration and astrobiology. *Sensors* 2006;6(6):688–696; doi: 10.3390/s6060688

Muramatsu H, Lam K, Bajusz C, et al. Lyophilization provides long-term stability for a lipid nanoparticle formulated, nucleoside-modified MRNA vaccine. *Mol Ther* 2022;30(5): 1941–1951; doi: 10.1016/j.ymthe.2022.02.001

Naumann D, Helm D, Labischinski H. Microbiological characterizations by FT-IR spectroscopy. *Nature* 1991;351(6321): 81–82; doi: 10.1038/351081a0

Okazaki R, Marty B, Busemann H, et al. Noble gases and nitrogen in samples of asteroid Ryugu record its volatile sources and recent surface evolution. *Science* 2023;379(6634):eabo0431; doi: 10.1126/science.abo0431

Pagès A, Grice K, Welsh DT, et al. Lipid biomarker and isotopic study of community distribution and biomarker preservation in a laminated microbial mat from Shark Bay, Western Australia. *Microb Ecol* 2015;70(2):459–472; doi: 10.1007/s00248-015-0598-3

Papineau D, She Z, Dodd MS. Chemically oscillating reactions during the diagenetic oxidation of organic matter and in the formation of granules in late Palaeoproterozoic chert from Lake Superior. *Chem Geol* 2017;470:33–54; doi: 10.1016/j.chemgeo.2017.08.021

Papineau D, Yin J, Devine KG, et al. Chemically oscillating reactions during the diagenetic formation of Ediacaran siliceous and carbonate botryoids. *Minerals* 2021;11(10):1060; doi: 10.3390/min11101060

Papineau D. Chemically oscillating reactions in the formation of botryoidal malachite. *Am Mineral* 2020;105(4):447–454; doi: 10.2138/am-2020-7029

Patel MR, Bérces A, Kerékgyárto T, et al. Annual solar UV exposure and biological effective dose rates on the martian surface. *Adv Space Res* 2004;33(8):1247–1252; doi: 10.1016/j.asr.2003.08.036

Patel MR, Zarnecki JC, Catling DC. Ultraviolet radiation on the surface of Mars and the Beagle 2 UV sensor. *Planet Space Sci* 2002;50(9):915–927; doi: 10.1016/S0032-0633(02)00067-3

Pavlov AA, Vasilyev G, Ostryakov VM, et al. Degradation of the organic molecules in the shallow subsurface of Mars due to irradiation by cosmic rays. *Geophys Res Lett* 2012;39(13); doi: 10.1029/2012GL052166

Png GM, Choi JW, Ng BWH, et al. The impact of hydration changes in fresh bio-tissue on thz spectroscopic measurements. *Phys Med Biol* 2008;53(13):3501–3517; doi: 10.1088/0031-9155/53/13/007

Poch O, Noblet A, Stalport F, et al. Chemical evolution of organic molecules under Mars-like UV radiation conditions simulated in the laboratory with the "Mars Organic Molecule Irradiation and Evolution" (MOMIE) setup. *Planet Space Sci* 2013;85:188–197; doi: 10.1016/j.pss.2013.06.013

Power IM, Wilson S, Thom JM, et al. The hydromagnesite playas of Atlin, British Columbia, Canada: A biogeochemical model for CO_2 sequestration. *Chem Geol* 2009;260(3–4): 286–300; doi: 10.1016/j.chemgeo.2009.01.012

Preston LJ, Barcenilla R, Dartnell LR, et al. Infrared spectroscopic detection of biosignatures at Lake Tírez, Spain: Implications for Mars. *Astrobiology* 2020;20(1):15–25; doi: 10.1089/ast.2019.2106

Preston LJ, Johnson D, Cockell CS, et al. Fourier transform infrared spectral detection of life in polar subsurface environments and its application to Mars exploration. *Appl Spectrosc* 2015;69(9):1059–1065; doi: 10.1366/14-07843

Preston LJ, Jungblut AD, Montgomery W, et al. The preservation and spectral detection of historic museum specimen microbial mat biosignatures within martian dust: Lessons learned for Mars exploration and sample return. *Astrobiology* 2024;24(7):684–697; doi: 10.1089/ast.2023.0118

Preston LJ, Melim LA, Polyak VJ, et al. Infrared spectroscopic biosignatures from Hidden Cave, New Mexico: Possible applications for remote life detection. *Geomicrobiol J* 2014; 31(10):929–941; doi: 10.1080/01490451.2014.913096

Riding R. Microbial carbonates: The geological record of calcified bacterial–algal mats and biofilms. *Sedimentology* 2000; 47(s1):179–214; doi: 10.1046/j.1365-3091.2000.00003.x

Rontó G, Bérces A, Lammer H, et al. Solar UV irradiation conditions on the surface of Mars. *Photochem Photobiol* 2003; 77(1):34–40.

Russell MJ, Ingham JK, Zedef V, et al. Search for signs of ancient life on Mars: Expectations from hydromagnesite microbialites, Salda Lake, Turkey. *JGS* 1999;156(5):869–888; doi: 10.1144/gsjgs.156.5.0869

Savijärvi HI, Martinez GM, Harri A-M. Surface energy fluxes and temperatures at Jezero Crater, Mars. *JGR Planets* 2023; 128(2):e2022JE007438; doi: 10.1029/2022JE007438

Scheller EL, Swindle C, Grotzinger J, et al. Formation of magnesium carbonates on earth and implications for Mars. *J Geophys Res Planets* 2021;126(7):e2021JE006828; doi: 10.1029/2021JE006828

Schopf JW, Farmer JD, Foster IS, et al. Gypsum-permineralized microfossils and their relevance to the search for life on Mars. *Astrobiology* 2012;12(7):619–633; doi: 10.1089/ast.2012.0827

Sharma VK, Klibanov AM. Moisture-induced aggregation of lyophilized DNA and its prevention. *Pharm Res* 2007;24(1): 168–175; doi: 10.1007/s11095-006-9138-7

Stalport F, Coll P, Szopa C, et al. Investigating the photostability of carboxylic acids exposed to Mars surface ultraviolet

radiation conditions. *Astrobiology* 2009;9(6):543–549; doi: 10.1089/ast.2008.0300

Stenberg B, Rossel RAV, Mouazen AM, et al. Visible and near infrared spectroscopy in soil science. *Advances in Agronomy* 2010;107:163–215; doi: 10.1016/S0065-2113(10)07005-7

Stuart BH. *Infrared Spectroscopy: Fundamentals and Applications*. John Wiley & Sons: Chichester, UK; 2004.

Turvey CC, Wilson S, Hamilton JL, et al. Hydrotalcites and hydrated Mg-carbonates as carbon sinks in serpentinite mineral wastes from the Woodsreef chrysotile mine, New South Wales, Australia: Controls on carbonate mineralogy and efficiency of CO_2 air capture in mine tailings. *Int J Greenhouse Gas Control* 2018;79:38–60; doi: 10.1016/j.ijggc.2018.09.015

Vago JL, Westall F, Coates AJ, et al.; Landing Site Selection Working Group Pasteur Instrument Teams, and Other Contributors. Habitability on early Mars and the search for biosignatures with the ExoMars rover. *Astrobiology* 2017;17(6–7): 471–510; doi: 10.1089/ast.2016.1533

Vasconcelos C, McKenzie JA, Bernasconi S, et al. Microbial mediation as a possible mechanism for natural dolomite formation at low temperatures. *Nature* 1995;377(6546):220–222; doi: 10.1038/377220a0

Viscarra Rossel RA, Cattle SR, Ortega A, et al. *In situ* measurements of soil colour, mineral composition and clay content by Vis-NIR spectroscopy. *Geoderma* 2009;150(3–4):253–266; doi: 10.1016/j.geoderma.2009.01.025

Visscher PT, Stolz JF. Microbial mats as bioreactors: Populations, processes, and products. In *Geobiology: Objectives, Concepts, Perspectives*. Elsevier: Amsterdam, 2005; pp. 87–100.

Whiting ML, Li L, Ustin SL. Predicting water content using Gaussian model on soil spectra. *Remote Sens Environ* 2004; 89(4):535–552; doi: 10.1016/j.rse.2003.11.009

Wood WW, Sanford WE. Ground-water control of evaporite deposition. *Econ Geol* 1990;85(6):1226–1235; doi: 10.2113/gsecongeo.85.6.1226

Xu Y, Chen S, Parlak O, et al. Discovery of extremely high-Al podiform chromitites from the Lycian (Marmaris) Ophiolite, SW Turkey: Implications for chromitite genesis. *Ore Geol Rev* 2020;127:103817; doi: 10.1016/j.oregeorev.2020.103817

Yılmaz B, Unsalan O. Raman spectroscopic assessment of hydromagnesite from Salda Lake. In: *53rd Lunar and Planetary Science Conference*. Lunar and Planetary Institute: Houston; 2022; abstract 1503.

Yin X, Weitzel F, Jimenez-Lopez C, et al. Directing effect of bacterial extracellular polymeric substances (EPS) on calcite organization and EPS–carbonate composite aggregate formation. *Cryst Growth Des* 2020;20(3):1467–1484; doi: 10.1021/acs.cgd.9b01113

Zedef V, Russell M, Fallick AE, et al. Genesis of vein stockwork and sedimentary magnesite and hydromagnesite deposits in the ultramafic terranes of southwestern Turkey: A stable isotope study. *Econ Geol* 2000;95(2):429–445; doi: 10.2113/gsecongeo.95.2.429

Zent AP. On the thickness of the oxidized layer of the martian regolith. *J Geophys Res* 1998;103(E13):31491–31498; doi: 10.1029/98JE01895

Zhang M, Oldenhof H, Sydykov B, et al. Freeze-drying of mammalian cells using Trehalose: Preservation of DNA integrity. *Sci Rep* 2017;7(1):6198; doi: 10.1038/s41598-017-06542-z

Zhang X, Zeng Y, Li Z. Enhanced hydromagnesite process for CO_2 sequestration by desilication of serpentine ore in NaOH solution. *Ind Eng Chem Res* 2020;59(25):11370–11380; doi: 10.1021/acs.iecr.0c01600

Zorzano M-P, Martínez G, Polkko J, et al. Present-day thermal and water activity environment of the Mars sample return collection. *Sci Rep* 2024;14(1):7175; doi: 10.1038/s41598-024-57458-4

Address correspondence to:
Connor J. Ballard
Department of Space and Climate Physics
Mullard Space Science Laboratory (MSSL)
University College London
Holmbury Hill Road
Dorking RH5 6NT
UK

E-mail: connor.ballard.21@ucl.ac.uk

Submitted April 4, 2025
Accepted January 8, 2026
Associate Editor: Kathleen A. Campbell